THE JOURNAL OF BIOLOGICAL CHEMISTRY VOL. 290, NO. 11, pp. 7097–7113, March 13, 2015
Published in the U.S.A.

Conditional Knock-out Reveals a Requirement for *O*-Linked *N*-Acetylglucosaminase (*O*-GlcNAcase) in Metabolic Homeostasis*

Received for publication, October 11, 2014, and in revised form, January 12, 2015 Published, JBC Papers in Press, January 16, 2015, DOI 10.1074/jbc.M114.617779

Chithra Keembiyehetty[‡], Dona C. Love[‡], Katryn R. Harwood[‡], Oksana Gavrilova[§], Marcella E. Comly[‡], and John A. Hanover[‡1]

From the [‡]Laboratory of Cell Biology and Biochemistry and [§]Mouse Metabolic Core Laboratory, NIDDK, National Institutes of Health, Bethesda, Maryland 20892

Background: The physiological functions of the *O*-GlcNAcase in development and metabolism are unclear.
Results: Conditional disruption of the *O*-GlcNAcase in mice leads to metabolic deregulation and semi-penetrant perinatal lethality.
Conclusion: Murine *O*-GlcNAcase maintains metabolic homeostasis and is particularly important during pregnancy and the postpartum period of development.
Significance: The findings reported here suggest a general role for OGA in the overall maintenance of metabolic homeostasis.

O*-GlcNAc cycling is maintained by the reciprocal activities of the *O*-GlcNAc transferase and the *O*-GlcNAcase (OGA) enzymes. *O*-GlcNAc transferase is responsible for *O*-GlcNAc addition to serine and threonine (Ser/Thr) residues and OGA for its removal. Although the *Oga* gene (*MGEA5*) is a documented human diabetes susceptibility locus, its role in maintaining insulin-glucose homeostasis is unclear. Here, we report a conditional disruption of the *Oga* gene in the mouse. The resulting homozygous *Oga* null (KO) animals lack OGA enzymatic activity and exhibit elevated levels of the *O*-GlcNAc modification. The *Oga* KO animals showed nearly complete perinatal lethality associated with low circulating glucose and low liver glycogen stores. Defective insulin-responsive GSK3β phosphorylation was observed in both heterozygous (HET) and KO *Oga* animals. Although *Oga* HET animals were viable, they exhibited alterations in both transcription and metabolism. Transcriptome analysis using mouse embryonic fibroblasts revealed deregulation in the transcripts of both HET and KO animals specifically in genes associated with metabolism and growth. Additionally, metabolic profiling showed increased fat accumulation in HET and KO animals compared with WT, which was increased by a high fat diet. Reduced insulin sensitivity, glucose tolerance, and hyperleptinemia were also observed in HET and KO female mice. Notably, the respiratory exchange ratio of the HET animals was higher than that observed in WT animals, indicating the preferential utilization of glucose as an energy source. These results suggest that the loss of mouse OGA leads to defects in metabolic homeostasis culminating in obesity and insulin resistance.

To date, ~1,000 proteins have been determined to possess the *O*-GlcNAc modification (1–4). Furthermore, OGT[2] and OGA have been found to be ubiquitously expressed in all tissues examined, exhibiting the highest levels in brain, pancreas and placenta (5–7). It is thought that the *O*-GlcNAc modification can alter protein function and downstream signaling in a manner that is analogous to protein phosphorylation (1, 3, 8–10). Because the substrate of OGT, uridine diphosphate *N*-acetylglucosamine (UDP-GlcNAc), is derived from the hexosamine biosynthetic pathway, which utilizes glucose, glutamine, acetyl CoA, and uridine diphosphate (UDP) to synthesize UDP-GlcNAc, it is thought that *O*-GlcNAc cycling may regulate cellular and metabolic processes in response to nutritional status, integrating multiple signaling pathways simultaneously. As such, substrate availability may be directly responsive to nutrient levels and consequently modulate protein *O*-GlcNAcylation status to, in turn, fine-tune metabolic status (8, 11, 12). Furthermore, it is likely that the extensive cross-talk between the phosphorylation and *O*-GlcNAcylation of proteins' serine and threonine residues could facilitate the concurrent modulation of multiple pathways in a nutrient-dependent manner (1, 8, 9).

Although *Oga* was first identified as the meningioma expressed antigen 5 (*Mgea5*) (13, 14), it was subsequently shown to be an *O*-GlcNAc-selective hexosaminidase with a neutral pH optimum (6, 15). Mammalian *Oga* is a highly conserved gene that is present as a single genomic copy located on human chromosome 10 (cytological position 10q24.1). The mouse *Mgea5* gene encoding *Oga* is located on chromosome 19 and contains 16 exons spanning ~31.5 kb (Fig. 1*A*). Several *Oga* splice variants have been detected, and these isoforms are differentially targeted within the cell (14, 16, 17). Furthermore, the *Oga* gene has been identified as a diabetes susceptibility locus in humans due to the fact that multiple single nucleotide polymorphism (SNP) sites of *Oga* are associated with an increased incidence of late onset diabetes among Mexican Americans

* This work was supported, in whole or in part, by a National Institutes of Health Intramural Grant.
[1] To whom correspondence should be addressed: LCBB, NIDDK, National Institutes of Health, 8 Center Dr., Bethesda, MD 20892. Tel.: 301-496-0943; Fax: 301-946-9431; E-mail: jah@helix.nih.gov.
[2] The abbreviations used are: OGT, *O*-GlcNAc transferase; OGA, *O*-GlcNAcase; HET, heterozygous; MEF, mouse embryonic fibroblast; HFD, high fat diet; RER, respiratory exchange ratio; HBP, hexosamine biosynthetic pathway; FDGlcNAc, fluorescein di(*N*-acetyl-β-D-glucosaminide); BisTris, 2-[bis(2-hydroxyethyl)amino]-2-(hydroxymethyl)propane-1,3-diol; ANOVA, analysis of variance; PAS, periodic acid-Schiff; T-PER, tissue protein extraction reagent.

(18–20). In addition, "Goto kakizaki" (GK) rats, which have a deletion at exon 8 in the *Oga* gene residing in chromosome 1, exhibit spontaneous diabetes (21).

Overall, it is known that perturbations in *O*-GlcNAc cycling impact chronic metabolic diseases such as diabetes, neurodegenerative disease, and cancer (3, 8, 11, 15, 22–25). These disease states may be a result of deregulated transcriptional machinery, as these perturbations in *O*-GlcNAc cycling likely alter the *O*-GlcNAcylation status of many proteins that are known to be modified, including transcription factors, histones, and RNA polymerase II (1, 3, 9, 12, 26, 27). Interestingly, mammalian *Ogt* is an X-linked, single copy gene that was shown to be essential for mouse embryonic stem cell viability (8, 28–32). Furthermore, studies using tissue-specific *Ogt* ablation in mice demonstrated the importance of the *O*-GlcNAc modification for normal tissue development and function (29).

Despite what has been shown previously, detailed analysis of the role of *O*-GlcNAcylation can be complicated due to the dynamic nature of the modification and the lack of a representative mammalian model system. However, several invertebrate models with altered *O*-GlcNAc cycling have been explored previously. Specifically in *Caenorhabditis elegans*, *ogt-1*- and *oga-1*-deficient mutants were found to be both viable and fertile but demonstrated alterations in longevity, dauer formation, macronutrient storage, and stress response (26, 33–39). In *Drosophila, Ogt* is known to be allelic to *super sex combs (Sxc*), the mutation of which results in a homeotic phenotype (40–42) and insulin signaling defects (25, 43). Although these models have provided valuable insights into the function of *O*-GlcNAc cycling in invertebrates, it remains unclear how well this is conserved in mammals.

The molecular roles of perturbations in *O*-GlcNAc cycling have been studied *in vitro* using several OGA inhibitors (44–47). This work has provided important information about the varied effects of altered *O*-GlcNAc cycling. However, these methods are limited by the differing specificity of the available OGA inhibitors. Inhibitor treatments in tissue culture experiments may not accurately reflect systemic homeostasis or the complex signaling pathways present in an entire organism. As such, it is important to establish a model system to genetically dissect the potential functions of *O*-GlcNAcylation in an intact organism. Recently, Yang *et al.* (48) examined a targeted mouse *Oga* hypomorphic allele generated by gene-trap technology. These authors reported both genomic instability and cell cycle-specific age-related effects of *O*-GlcNAc cycling perturbations using MEFs derived from these animals. They also noted that *O*-GlcNAcase heterozygosity suppressed intestinal tumorigenesis (49). Unfortunately, although informative, the gene-trap approach is limited in that it often produces hypomorphic rather than null alleles and also cannot produce conditional knock-out alleles; these facts encouraged us to adopt alternative approaches.

In this study, we employed a Cre-*loxp*-based conditional deletion strategy targeting the promoter and exon 1 of the *Oga* gene to create a conditional null allele (50, 51). Here, we describe methods to elucidate the metabolic effects of OGA deletion using our newly developed model system, both in MEF cells derived from HET and KO animals and in adult mice. In these studies, we find that *Oga* null pups exhibit a high incidence of neonatal lethality associated with low glycogen stores and hypoglycemia. We also observe that total GSK3β expression is altered in both KO MEFs and mouse tissue, although the GSK3β phosphorylation-dependent insulin response is altered in KO MEF cells alone. HET mice show elevated RER consistent with the preferential utilization of carbohydrate as opposed to fat as an energy source. Furthermore, metabolic analysis shows that HET females possess increased fat mass, reduction in insulin sensitivity, and other hallmarks of metabolic syndrome.

MATERIALS AND METHODS

Floxed Construct with OGA Gene Targeting—The floxed *Oga* construct was designed to delete exon 1 to produce *Oga* null mice devoid of all splice isoforms. The ~10.5-kb region used to construct the targeting vector (pGKNeo cassette) was first subcloned from a positively identified B6 BAC clone using homologous recombination (inGeneious Targeted Laboratory Inc., Ronkonkoma, NY). The single *loxP* site and a unique restriction digestion site (EcoRI) were inserted upstream of exon 1, allowing diagnostic identification of the floxed allele. The *loxP/FRT*-flanked *neo* cassette (~8.0 kb long) was inserted downstream of exon 1. The target region was ~1.1 kb, including exon 1. The target vector was linearized by NotI digestion and then transfected into C57Bl/6 embryonic stem cells by electroporation. After G418 selection, surviving clones were expanded for PCR analysis to identify recombinant embryonic stem (ES) cell clones. HET mice bearing a floxed *Oga* gene were derived from these ES cells. Seven founder (F0) mice bearing this construct were identified by screening for the inserted DNA by PCR amplification and sequencing of a 2.7-kb fragment. HET *Oga* floxed mice ($Oga^{floxed/+}$) were housed at the animal facility at the National Institutes of Health, and experiments were conducted according to the National Institutes of Health guidelines for animal care and use protocols. They were fed *ad libitum* a normal chow diet and water. Pregnant and newborn pups were given access to a high energy (high lipid) soft diet. $Oga^{floxed/+}$ were cross-bred to generate KO floxed chimera mice ($Oga^{floxed/floxed}$). Pups were weaned after 3 weeks and genotyped using tail DNA (see below). Although more than 50 littermates from three breeding pairs were monitored and tested, no live births of KO *Oga* floxed pups were detected. For embryos with the *Oga* floxed KO gene, normal size was observed at embryonic day 12.5.

As an alternative breeding strategy, HET *Oga* floxed male mice ($Oga^{floxed/+}$) were cross-bred with the murine mammary tumor virus-Cre female mice to derive *Oga* HET mice. This female murine mammary tumor virus-LTR line A mouse expressing Cre recombinase in the oocytes was a kind gift from Dr. L. Hennighausen's laboratory (NIDDK, National Institutes of Health). Details of the Cre expression pattern in this (line A) mouse have been described previously (83). The resultant F1 generation littermates were genotyped using the PCR protocol developed to identify the deletion of *Oga* as described below. These crosses generated eight *Oga* HET pups, some of which also possessed deletions in the *neo* gene. *Oga* HET mice were selected and cross-bred to generate *Oga* KO mice lacking the

neo cassette. The Cre allele was detected by the presence of a lighter coat color in the Cre-positive animals.

Cross-breeding of these *Oga* HET littermates did not produce any *Oga* KO offspring in the F2 generation. After monitoring several breeding pairs and screening more than 400 pups, we were unable to find any surviving *Oga* KO animals. We subsequently examined multiple embryonic stages and noted that despite their lack of post-embryonic survival, *Oga* KO embryos do in fact to appear to be viable until birth.

PCR Genotyping Protocols—DNA was extracted from the mouse tails as described by Miller *et al.* (84). The genotyping PCR primers used were as follows: (*a*) forward primer OGA-UTR1F 5′-ACC GCA CAC TCT CCA TCG CCA TAA-3′; (*b*) reverse primer 1 OGA-UTR4R 5′-CCC GCT TCC TGT TTA TCC GCA CTG-3′; and (*c*) reverse primer 2 OGAR7 5′-CAC CGC CTC CTC CTC CGA CAA ATC-3′. PCRs were performed in an Eppendorf master cycler using the hot start *Taq* polymerase (TaKaRa) enzyme. About 50 ng of DNA was used in 20-μl reactions with 80 pmol of dNTP mixture and 10 pmol of each primer. PCR amplification was performed after 1 min of 94 °C heat inactivation followed by cycle conditions of 94 °C denaturing for 30 s, 60 °C annealing for 30 s, and 72 °C extension for 3 min, repeating 35 cycles with a final extension reaction for 5 min at 72 °C. (This primer set was designed to yield a unique banding pattern for WT (750 bp), HET (550 and 750 bp), and KO (550 bp) *Oga* deletion.) Another PCR was performed to detect the presence of exon 1 using the primer pair OGAEX1F (5′-GCCCCCGCCGAGAGGAA-3′) and OGAEX2R (5′-CCAC-GACACCGCACAGGA-3′) located in the exon 1 region. The reaction conditions included an incubation at 94 °C for 20 s, 60 °C for 20 s, and 72 °C for 30 s, repeating 30 cycles and ending the reaction with a 5-min extension at 72 °C. The product of this PCR is a 300-bp product in WT and HET animals with no band detectable in KO animals. Using the reaction procedure described above, the presence of the *neo* cassette was identified by a PCR using the primer pair forward 5′ 5′-TGC TCC TGC CGA GAA AGT ATC CAT CAT GGC and reverse 5′-CGC CAA GCT CTT CAG CAA TAT CAC GGG TAG at 29 cycles. This PCR yields a 390-bp product in animals possessing the *neo* gene.

Embryonic Studies—Embryos at different developmental stages were collected at 13.5, 16, and 18 days. Tail DNA was used for genotyping. Both fetuses and placentas of 16- and 18-day-old fetuses were fixed in Bouin's reagent for histopathological examinations. Samples were processed and embedded in paraffin at the NCI core facility (Frederick, MD). Subsequent sagittal sections of these fetuses and placenta were stained with hematoxylin/eosin and examined at the same facility.

MEF Isolation—MEFs were collected at embryonic days 12.5–13 following the protocol from Fred Hutchinson Cancer Center. Cells were cultured in DMEM supplied with 10% FBS, 100 units/ml penicillin, and 100 μg/ml streptomycin. Cells were frozen under liquid nitrogen at passage 1–3 in 7% DMSO and 20% FBS for future use. Cells were analyzed to confirm *Oga* mRNA and protein expression patterns as described below.

mRNA and Protein Analysis—To evaluate the whole body expression in *Oga* KO mice, tissue and MEF cells were examined for mRNA expression by semi-quantitative RT-PCR. The total RNA was isolated from the tissue using TRIzol reagent (Invitrogen). DNase digestion was performed (Qiagen), and the products were purified using the RNeasy mini kit according to the manufacturer's instructions. cDNA was synthesized from 5 μg of total RNA using Superscriptase III (Invitrogen) in a 20-ml reaction volume according to the enzyme supplier's instructions. The final reaction was diluted to 100 μl, and semi-quantitative PCR was performed in a 20-μl reaction mixture containing 2 μl of cDNA, using HS TaqDNA polymerase (TaKaRa). The following primer pairs were used for amplifying mouse OGA: long isoform (*a*) sense 5′-TGTGCAGTGGTTAGGGTGTC-3′ and (*b*) antisense 5′-GAAGGGAAGTTGGCAAGGAAAGTT-3′, and for the short isoform (*a*) sense 5′-GGCAAATTTCCATG-TTCTTCAG-3′ and (*b*) antisense 5′-ACCCCGTTGCAGTC-TTTGTG-3′. 18 S rRNA was used as a control and was amplified using the following primers: (*a*) forward 5′-CCCGGGGA-GGTAGTGACGAAAAAT-3′ and (*b*) reverse 5′-CGCCCGC-TCCCAAGATCCAACTAC-3′. The reaction mixture was denatured at 94 °C for 1 min and amplified using 30 cycles for the OGA isoforms and 24 cycles for the 18 S rRNA fragment. The cycling conditions for all reactions consisted of a 30-s 94 °C denaturing step, a 30-s 56 °C annealing step, and a 30-s 72 °C polymerization step, followed by a single 5-min extension at 72 °C.

O-GlcNAcylated protein levels in each group were examined by Western blotting using two anti-*O*-GlcNAc antibodies (RL2 (MA1-072: Affinity Bio Reagents, CO) and CTD110.6 (Covance, CA)). Liver samples were excised from euthanized mice and immediately frozen in liquid nitrogen and stored at −80 °C. Tissue samples were processed using glass homogenizers and the addition of 1:5 (w/v) of T-PER lysis buffer (Pierce) with cOmplete EDTA-free protease inhibitor mixture and phosSTOP (both from Roche Applied Science) added per the manufacturers' recommendations. Lysates were clarified by centrifugation at 5,000 × *g* for 10 min at 4 °C. The lysate was further homogenized by 20 passages through a 25-gauge syringe, and the resultant material was pelleted at 14,000 × *g* for 10 min. Protein concentration was determined using a BCA assay (Pierce). Equal amounts (50 μg) of protein were boiled with sample buffer (LDS, Invitrogen) for 10 min and resolved using precast NUPAGE BisTris mini gels (10% and 1.5 mm thickness) using MOPS buffer. Gels were transferred to a nitrocellulose membrane and blocked with Odyssey blocking buffer (LI-COR Biosciences). The blots were first probed with either anti-OGA (ProteinTech Group Inc., catalog no.14711-1-AP) or anti-OGT (Santa Cruz Biotechnology, catalog no.sc32921) primary antibodies and then fluorescent secondary antibodies (LI-COR Biosciences IRDye800-CS donkey anti-rabbit IgG catalog no. 926-32213 or IRD680-LT goat anti-mouse IgG catalog no. 926-32220) and were finally imaged using an Odyssey Infrared Imaging System (LI-COR Biosciences). For both OGA and OGT, actin levels were used as the loading control (anti-actin antibody Sigma, catalog no. A5441). Protein expression levels and the phosphorylation patterns of WT, HET, and KO MEFs were evaluated under basal and insulin-stimulated conditions (100 nM) using Western blot analysis. Total GSK3β and phospho-GSK3β Ser-9 antibodies were from Cell Signaling Technology (GSK, catalog no. 9332 and GSKβ3 Ser-9 catalog no. 9336S).

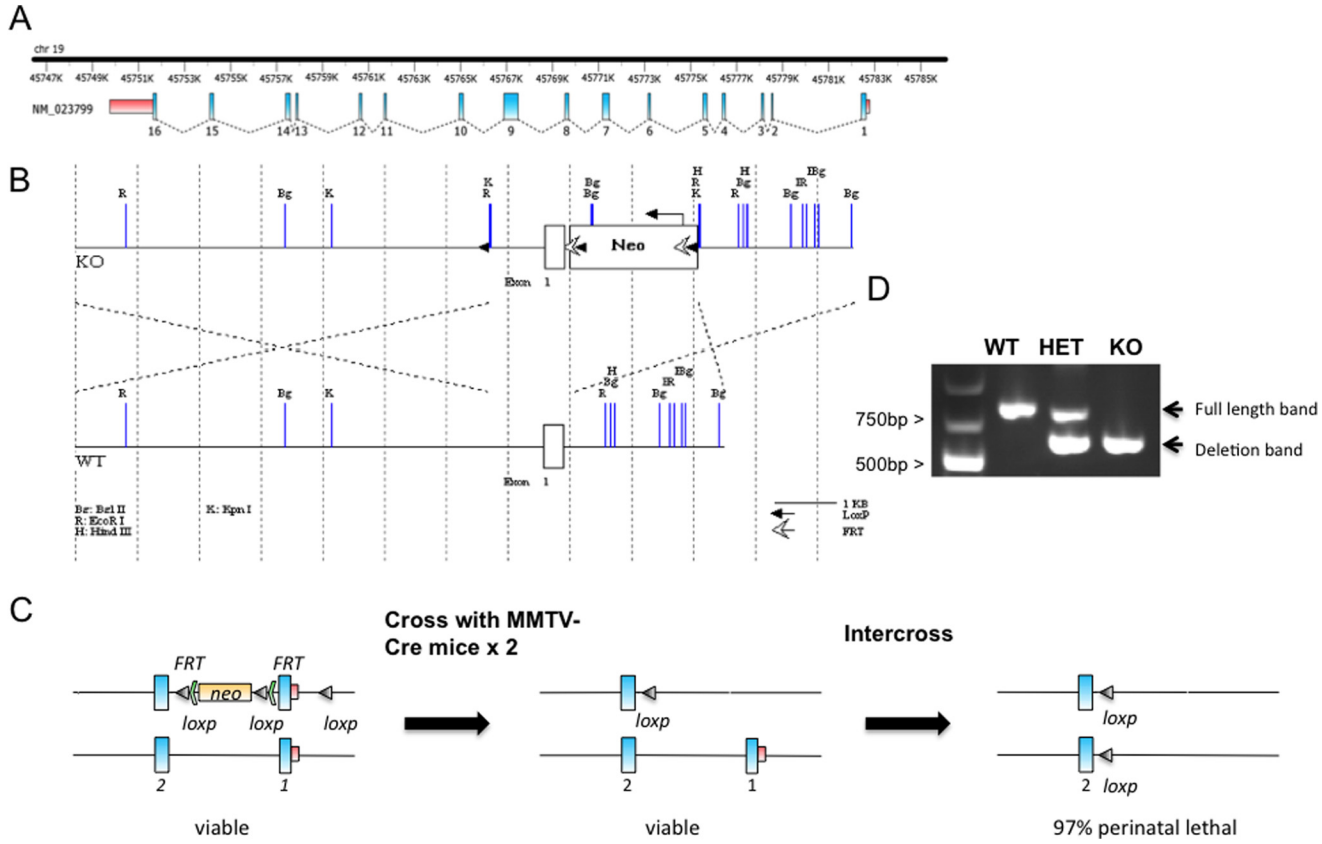

FIGURE 1. *A,* schematic diagram of the mouse *Oga* gene. *B,* Cre-*loxP* insertion strategy targeting *Oga* deletion at exon 1. *C,* breeding strategy employed to generate the *Oga* KO mice. Male chimeric mice bearing a floxed *Oga* allele were crossed with female MMTV-Cre mice expressing Cre in the oocyte in a two-step breeding strategy to remove both *neo* and floxed sites. HET *Oga* animals with a floxed *neo* cassette were intercrossed with siblings, resulting in *Oga* KO animals with 3% perinatal survival. *D,* PCR data confirming the *Oga* deletion status in HET and KO animals.

Microarray—Global gene expression profiles of WT and KO MEFs were investigated by microarray using Affymetrix array chips in triplicate. RNA was extracted as described above, and quality was tested in a BioAnalyzer (Agilent Technologies) using RNA6000 nano chips. High quality RNA extracted from female embryos from each genotype (WT, HET, and KO) was used to perform the microarray analysis. Affymetrix Mouse Genome 430 2.0 chips were used in technical triplicates for each genotype. cDNA prepared using Affymetrix kits according to the manufacturer's instruction was hybridized to the chips for 16–18 h at 45 °C. Chips were washed, stained, and scanned using the Affymetrix 3000 scanner. Data were normalized using a MAS5 algorithm and analyzed using Partek software. These data are deposited as Geo dataset GSE52721.

Metabolic Studies—Mice were reared three/four per cage on a 12-h light-dark cycle (lights on from 0600 to 1800) and fed water and NIH-07 diet (11% kcal fat, Zeigler Brothers, Inc., Gardners, PA) *ad libitum*. Mice were transferred to a D12492 HFD (60% kcal fat, Research Diets Inc., New Brunswick, NJ) at 17 weeks and were maintained on this diet for 10 weeks. Body weight and body composition were measured every other week. Energy expenditure, RER, food intake, and activity were measured by indirect calorimetry at 22 °C using a 12-chamber CLAMS system (Columbus Instruments, Columbus, OH) as described previously (66). Mice were acclimated for 2 days in the metabolic chamber before measurements were taken. After the 2-day acclimation, data were collected for 24 h. Day (light cycle) was from 0600 to 1800 h and night (dark cycle) was from 1800 to 0600 h.

Biochemical Assays to Determine Body Composition Analysis—Body composition was measured in nonanesthetized mice using the Echo3-in-1 NMR analyzer (Echo Medical Systems, Houston, TX). Blood was obtained from the tail veins of animals in the nonfasted state. Blood glucose levels were measured using Glucometer Contour (Bayer, Elkhart, IN). Serum or plasma insulin, leptin, and adiponectin were assayed using radioimmunoassay (Millipore/Linco Research, St. Charles, MO). Serum triglycerides and cholesterol and free fatty acid levels were measured according to the manufacturer's procedures (Thermo DMA, Louisville, CO, and Roche Applied Science).

Glucose and Insulin Tolerance Tests—Mice fasted overnight were used in the glucose tolerance assay. Glucose was injected intraperitoneally at 2 g/kg body weight in mice fed normal chow or 1 g/kg body weight in mice fed a HFD. Blood glucose levels were measured at 0, 15, 30, 60, and 120 min after injection. Additionally, 20 μl of blood samples were collected from these mice at 0, 15, and 120 min to evaluate plasma insulin concentration. For insulin tolerance tests, nonfasted mice were injected intraperitoneally with human insulin (Humulin R; Lilly) at 0.75 IU/kg body weight. Blood glucose levels were measured at 0, 15, 30, 45, 60, 90, and 120 min after injection.

Liver Glycogen Analysis—Liver glycogen was detected in liver sections embedded into paraffin by American Histolabs (Gaith-

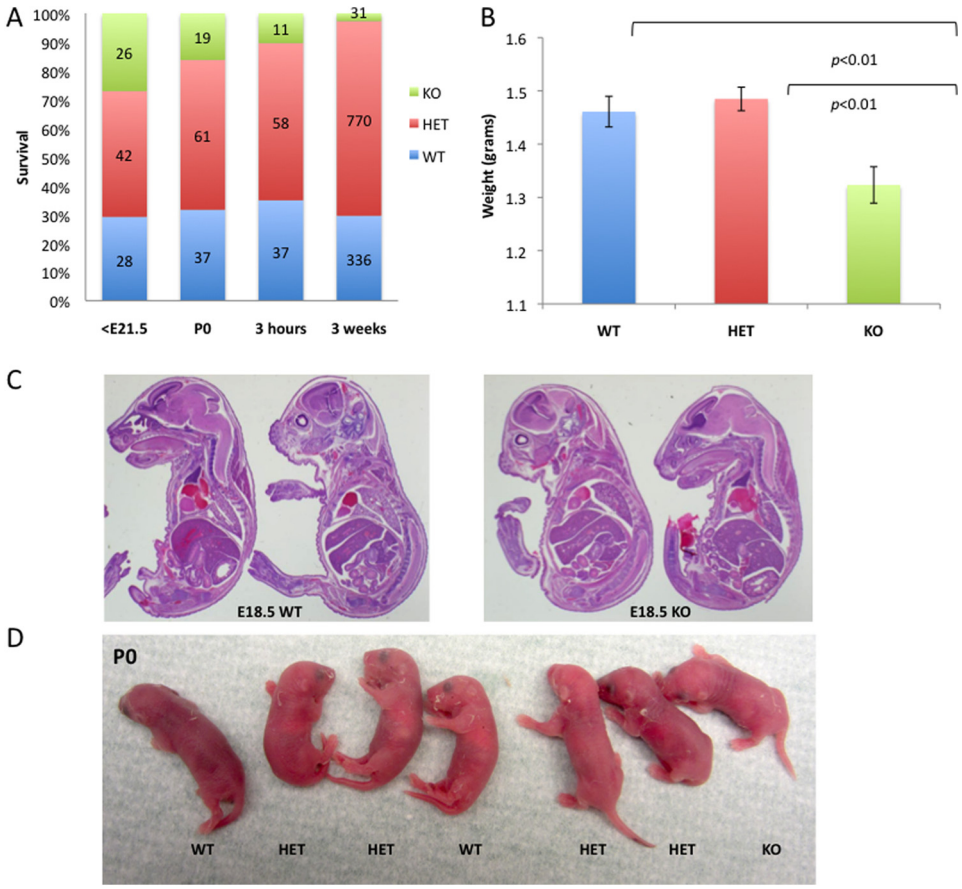

FIGURE 2. **Deletion of *Oga* is perinatal lethal.** ***A,*** survival of *Oga* KO animals compared with their HET and WT littermates at indicated time points. Numbers of each genotype are indicated on the *graph*. *B,* weight distribution (in grams) of pups of each genotype at birth (WT $n = 31$, HET $n = 52$, and KO $n = 16$). P0 *Oga* KO animals are significantly smaller than their WT or HET littermates. *C,* histological examination of hematoxylin and eosin-stained sagittal sections from WT and KO embryos at E18.5 did not reveal any gross developmental defects. *D,* live pups at P0 (birth). Genotypes are shown *below* each pup. Note that the *Oga* KO pup shows normal color and no sign of respiratory distress compared with its WT and KO littermates.

ersburg, MD). Kidney histology was examined after periodic acid-Schiff (PAS) staining.

O-GlcNAcase Activity Assay—WT, HET, and KO MEFs were lysed in T-PER (Pierce) with cOmplete EDTA-free protease inhibitor mixture (Roche Applied Science) added fresh by rocking gently at 4 °C for 10 min and clarifying by centrifugation. 30 μg of clarified lysate was added to a mixture of 200 μM fluorescein di(*N*-acetyl-β-D-glucosaminide) (FDGlcNAc) and 50 mM *N*-acetylgalactosamine (GalNAc), in 50 mM citrate/phosphate buffer, pH 6.5. To control for any background fluorescence of the FDGlcNAc substrate itself, T-PER was added to a mixture of FDGlcNAc and GalNAc in the citrate/phosphate buffer ("no lysate"). All reactions were incubated in the dark at 37 °C and shaken at 100 rpm for 30 min. The reactions were quenched by adding Na_2CO_3 to a final concentration of 400 mM. Fluorescence was measured in 1-s intervals at the excitation wavelength of 485 nm and at the emission wavelength of 535 nm on a Wallac 1420 fluorometer (PerkinElmer Life Sciences). All assays were performed in triplicate. For data analysis, the signal detected in the no lysate reactions was averaged, and this value was subtracted from each of the lysate measurements. Data are presented as the mean ± S.E.

Statistical Analysis—The experiments represented in Figs. 9–11 were performed using groups of 12 or more mice. One-way ANOVA tests were performed to determine significance and the mean ± S.E. Data are considered significant at $p \leq 0.05$ level as denoted by a single asterisk and $p \leq 0.01$ by a double asterisk.

RESULTS

Oga KO Mice Exhibit a Highly Penetrant Perinatal Lethal Phenotype—*Oga* exon 1 and its promoter were chosen for conditional deletion using a Cre-*loxP* strategy (Fig. 1, *B* and *C*). Initial breeding attempts to propagate chimeric mice bearing a homozygous *Oga* floxed allele were unsuccessful due to the retention of the *neo* cassette, as reported previously for other knock-out mouse studies (50, 51). To circumvent this problem, the null *Oga* allele was generated by crossing male chimeric mice bearing an *Oga* floxed allele with female mice expressing Cre in the oocyte (Fig. 1*C*). Genotypes were confirmed by PCR (Fig. 1*D*). We noted that mating of the HET animals produced only 3% KO pups at weaning. Genotypes obtained at embryonic stages and at birth confirmed that although KO embryos were present at the expected Mendelian inheritance ratio, they died soon after birth with relatively few surviving to 3 weeks (Fig. 2*A*). Although the KO pups had significantly lower weight at birth (Fig. 2*B*), we did not find any obvious developmental defects or gross structural defects associated with the KO allele by histopathological analysis of whole mount embryonic sections at day E18.5 (Fig. 2*C*). Furthermore, no structural defects

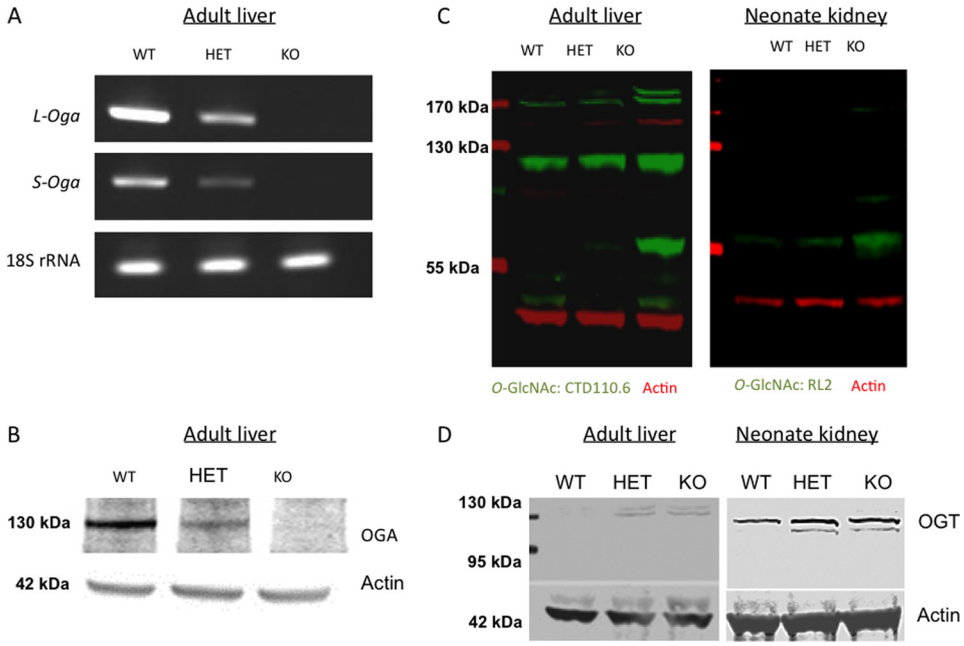

FIGURE 3. **OGA and OGT expression in transgenic tissues.** *A,* mRNA levels of the long and short isoforms of *Oga* in adult liver tissues from all genotypes. No mRNA transcript is produced in *Oga* null mice. Ribosomal 18 S rRNA (*lower panel*) was used as a control. *B,* Western blots probed with anti-OGA antibody demonstrate the loss of an immunoreactive band at 130 kDa, the expected size of the OGA protein, in KO tissue. This band is observed at intermediate levels in HET tissues. *C, Oga* deletion exhibited greatly increased *O*-GlcNAcylated protein levels as detected by anti-*O*-GlcNAc antibody (CTD110.6 antibody, *green channel*) in adult liver tissues (*left*) and newborn kidney (*right*, RL2 antibody *green channel*). HET tissues exhibit a slight increase in *O*-GlcNAcylation as compared with WT. Actin bands (*red channel*) show similar amounts of protein for all three genotypes. *D,* Western blot analysis of tissue derived from both adult liver and neonate kidney of HET and KO mice shows increased OGT levels as compared with that observed in tissue from WT mice. Standards on the *left* apply to both blots because they were derived from a single Western blot.

were detected at any stage of development examined (E13.5, E16.5, or E18.5) or in either HET or KO mutant animals. Other than the documented lower body weight, the KO pups were difficult to distinguish from WT or HET littermates (Fig. 2*D*).

Conditional Oga Deletion Leads to Loss of Oga mRNA, Protein, and Activity—The floxed *Oga* locus was expected to produce a null allele lacking all known *Oga* isoforms due to the fact that both the first coding exon and promoter elements were targeted for deletion (Fig. 1*A*). To confirm this, RNA isolated from livers of animals harboring the WT, HET, and KO deletions was analyzed by PCR (Fig. 3*A*). The two major *Oga* transcripts were absent in KO animals, and only intermediate levels were present in HET animals. Anti-OGA antibody was used to probe immunoblots of adult liver tissue, and this analysis confirmed the absence of OGA in KO tissues and its reduction in HET tissues (Fig. 3*B*). As a result of the *Oga* deletion, the global levels of protein *O*-GlcNAcylation were substantially increased in KO tissues (adult liver and neonatal kidney) as evidenced by Western blots probed with anti-*O*-GlcNAc antibody (Fig. 3*C*). We also examined OGT levels using Western blot analysis in WT, HET, and KO tissues. Interestingly, in both adult liver and neonate kidney tissues in HET and KO animals, OGT levels were observed to increase relative to that observed in WT animals (Fig. 3*D*).

Oga KO Perinatal Lethality Was Associated with Hypoglycemia—Although a few of the KO pups had milk spots, demonstrating their ability to feed, very few animals survived past 24–48 h after birth (Fig. 2, *A* and *D*). Notably, perinatal death of mutant mice has been linked to impaired physiological processes, including glucose homeostasis (52). To determine whether glucose homeostasis was impaired in *Oga* KO pups, we measured blood glucose levels of newborns at birth and after an 8-h fast. Interestingly, we found a higher incidence of hypoglycemia in KO neonates that was significantly different from their WT and HET littermates (Fig. 4*A*). Although WT and HET mice were able to maintain normal levels of circulating glucose during this time, the circulating glucose concentration in KO animals dropped to near undetectable levels (Fig. 4*A*). The impaired glucose homeostasis under fasting conditions in KO pups suggested either an inability to mobilize glycogen or depleted glycogen stores. To test this hypothesis, neonatal liver sections from WT and KO mice were stained by PAS to identify liver glycogen accumulation (Fig. 4*B*). Quantitation of PAS staining demonstrated a dramatic reduction in hepatic glycogen deposition in KO animals compared with WT animals (Fig. 4*C*). This reduction in liver glycogen pools in KO newborns suggests that the hypoglycemia may be linked to neonatal glucose homeostasis. Taken together, these findings suggest that KO animals are compromised in their ability to maintain insulin-glucose homeostasis, resulting in hypoglycemia and perinatal lethality.

Total O-GlcNAcylation of Proteins Increased in Oga KO MEF Cells—Employing a more defined *in situ* system, we prepared MEFs from gender-matched WT, HET, and KO siblings (12.5 days postcoitus). Each cell line was tested for *Oga* mRNA expression, OGA protein levels, and OGA enzymatic activity. As expected, transcripts encoding the two major *Oga* isoforms were absent in KO MEFs, although an intermediate level of expression was detected in HET MEFs (Fig. 5*A*). The loss of *Oga* transcript correlated with a proportional reduction in enzy-

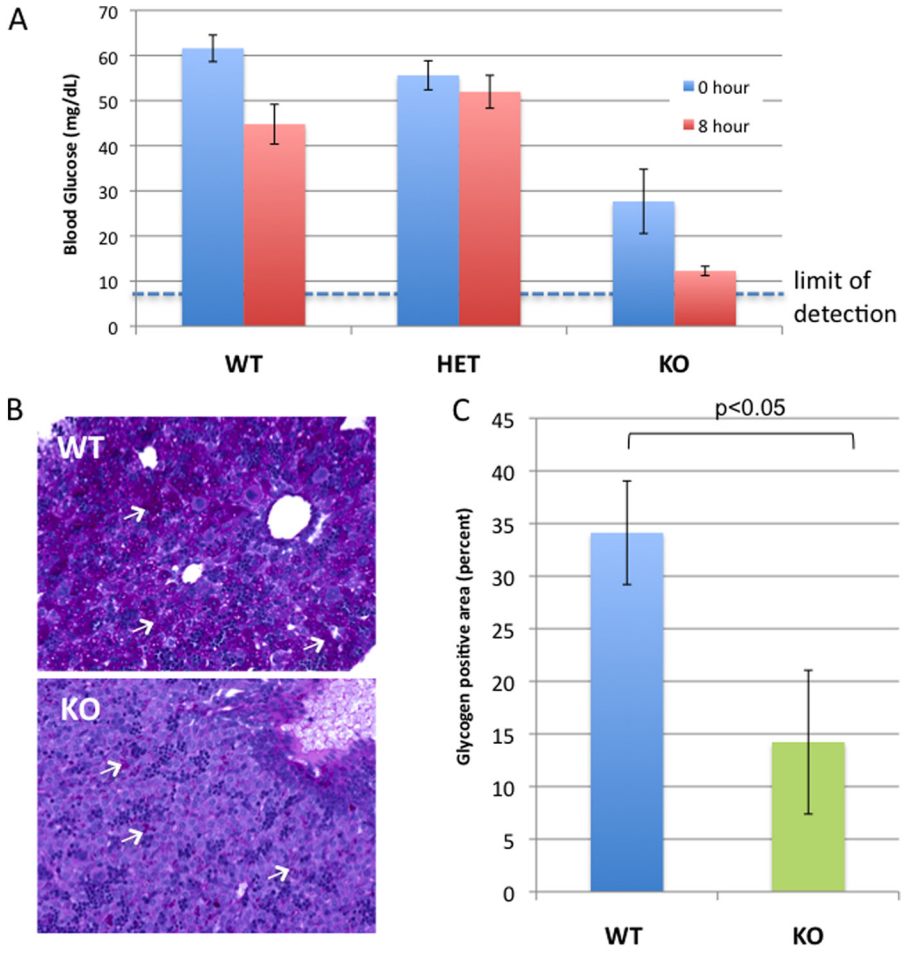

FIGURE 4. **Glucose homeostasis is impaired in *Oga* KO animals.** *A,* glucose levels from whole blood was measured for each genotype at birth (0 h) and after an 8-h fast. Data are presented as the mean ± S.E. The glucometer used had a detection limit of 10 mg/dl (*dashed line*). *B,* histological analysis of liver sections from P0 *Oga* WT and KO littermates. Sections were stained with hematoxylin/eosin, and glycogen content (noted with *white arrows*) was determined by PAS staining. *C,* graphed are the results of the imaging analysis. Glycogen content of KO livers was found to be significantly reduced compared with WT ($p < 0.05$). *Bars* represent the mean ± S.E. A total of four fields were measured for each liver (for each WT and KO $n = 5$).

matic activity as measured using the fluorescent OGA substrate FDGlcNAc (Fig. 5*B*) (53). Similarly, the total amount of protein *O*-GlcNAcylation in these cells was inversely correlated with the level of OGA as detected by anti-*O*-GlcNAc antibody (Fig. 5, *C* and *D*). Taken together, these findings suggest that the conditional *Oga* allele described herein is in fact a null allele that exhibits haploinsufficiency when paired with a WT allele (*i.e.* in HET animals).

Insulin-response Signaling through GSK3β Is Dramatically Altered in Oga KO Animals—Because we found that *Oga* deletion had a profound effect on glycogen mobilization in KO neonatal mice, we elected to examine which signaling pathways may be involved. Previous studies from our laboratory (54) and others (55) have linked *O*-GlcNAc cycling to insulin resistance. To examine the insulin response associated with *Oga* deletion, we evaluated MEF cells under basal and insulin-stimulated conditions. We examined a panel of key regulatory proteins in insulin signaling using Western blot analysis, including IRS1, AKT, PDK1, and AMPKα. One key protein that consistently emerged from this extensive analysis was GSK3β, which showed both increased expression and phosphorylation in the KO MEFs. Increased phosphorylation at Ser-9 in GSK3β was detected in MEF cells under basal conditions (Fig. 6*A*, *left*). In the presence of insulin, GSK3β phosphorylation increased in WT animals but remained the same in HET MEFs and decreased in KO MEFs (Fig. 6, *A* and *B*). To verify these findings *in vivo*, we examined total GSK3β expression levels in adult and neonatal livers. For both adult and neonatal liver, greatly enhanced levels of GSK3β were detected in KO animals with an intermediate increase in GSK3β HET liver tissues (Fig. 6, *C* and *D*). Previous studies have shown that overexpression of GSK3β leads to inhibition of both basal and insulin-stimulated glycogen synthase activity (56–58). Our findings suggest that the perinatal lethality and paucity of glycogen stored in neonatal livers observed in the KO animals may be linked to elevated GSK3β levels. Given the pleiotropic role of GSK3β in modulating Wnt signaling, glycogen metabolism, innate immunity, and insulin signaling (59), we then used whole genome transcriptional profiling to determine whether other pathways may have become deregulated.

Oga KO and HET MEFs Exhibit Changes in Metabolic Pathway Genes—RNA obtained from female *Oga* MEF cells derived from animals of all three genotypes was analyzed by microarray to identify global gene expression patterns associated with *Oga* deletion. Principal component analysis revealed distinctly separate gene expression in WT, HET, and KO groups (Fig. 7*A*).

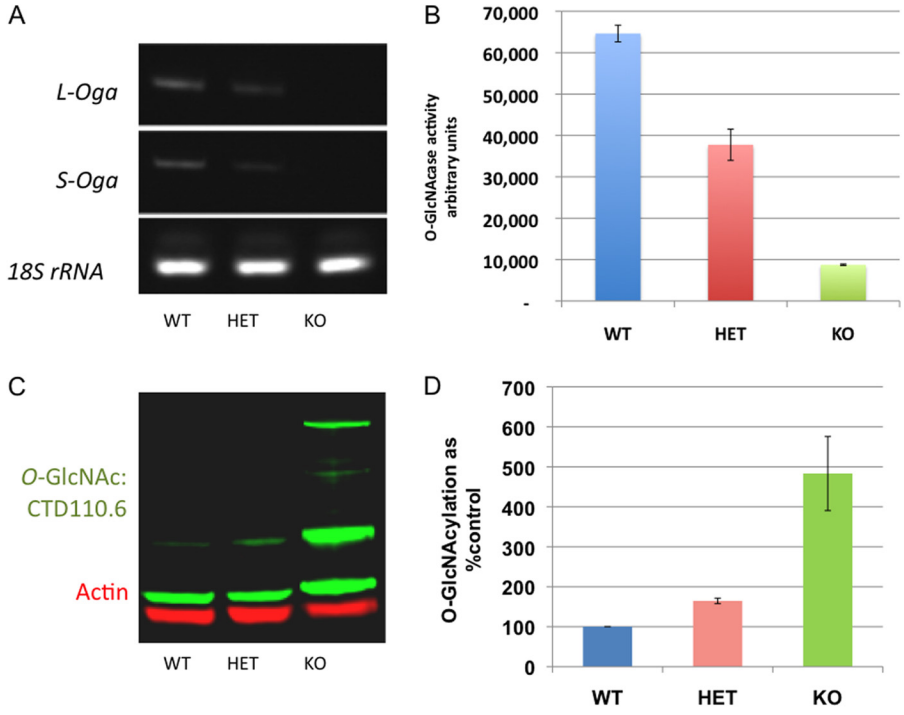

FIGURE 5. **Effects of *Oga* deletion in MEFs.** *A,* semi-quantitative RT-PCRs followed by gel electrophoresis show transcripts levels of long and short *Oga* isoforms were reduced in HET and absent in KO cells relative to WT. 18 S rRNA gene expression was used as a control. *B, O*-GlcNAcase activity was measured using the fluorogenic OGA substrate FDGlcNAc in MEF cells. HET cells exhibited intermediate OGA activity using this assay, and very little activity was observed in KO cells. Data are the mean ± S.E. *C,* representative Western blot showing increased *O*-GlcNAcylation in *Oga* KO MEF cells. Blots are probed with CTD110.6 antibody (*green channel*) and actin (*red channel*). The immunoblot is representative of what was observed in three independent experiments. *D,* graph of the quantification of the representative blot in *C* done over 5 logs on images taken on an Odyssey Infrared Imaging System (LI-COR Biosciences) shows notable increases in *O*-GlcNAc band intensity in KO cells (normalized to actin levels). *Error bars* represent ± S.E.

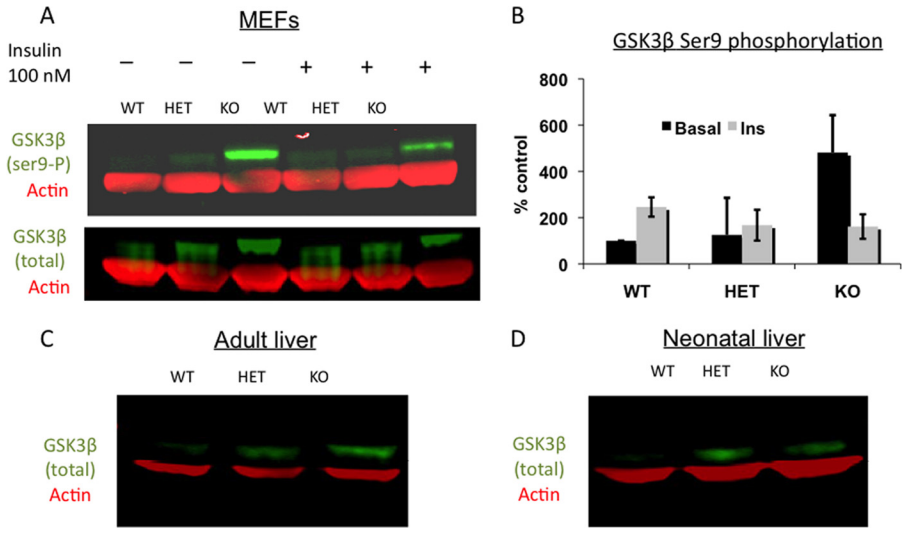

FIGURE 6. *A,* Western blots from MEF cells probed with GSK3β Ser(P)-9 (*Ser9-P*) or total GSK3β (*green*) and actin (*red*) antibodies show basal and insulin-mediated GSK3β Ser-9 phosphorylation increased in *Oga* KO MEF cells compared with WT cells (WT MEFs were from a female and both HET and KO MEFs from a male). *B, graph* showing both increased basal GSK3β phosphorylation in KO MEFs compared with WT MEFs and the notable insulin (*Ins*)-dependent reduction in phosphorylation levels observed specifically in KO MEFs. Densitometry data from two independent experiments are represented. Each of the GSK3β species was normalized first to actin alone, and then the ratio of GSK3β Ser(P)-9 to total GSK3β was determined. The WT ratio under basal conditions was set at 100%, and the other ratios are plotted as a percentage of this to evaluate both the GSK3β phosphorylation levels in the mutant lines and to determine phosphorylation changes upon insulin stimulation. Values are means ± S.E. *C* and *D,* Western blots showing total GSK3β expression in adults (all females) and newborn livers (WT and KO were each from a male and HET was from a female) corroborated MEF data. GSK3β expression increased in HET and KO mice tissues compared with WT.

Differentially expressed genes were calculated by ANOVA ($p < 0.05$) using Partek software. Genes that changed by at least 2-fold, up or down, were identified using a 0.01 false discovery ratio. Although KO MEFs had 838 transcripts that changed 2-fold or over compared with WT, comprising 619 unique transcripts with 36 unmapped transcripts, 111 transcripts were differentially expressed in the HET group with 82 unique transcripts and 22 unmapped transcripts. Hierarchical clustering of

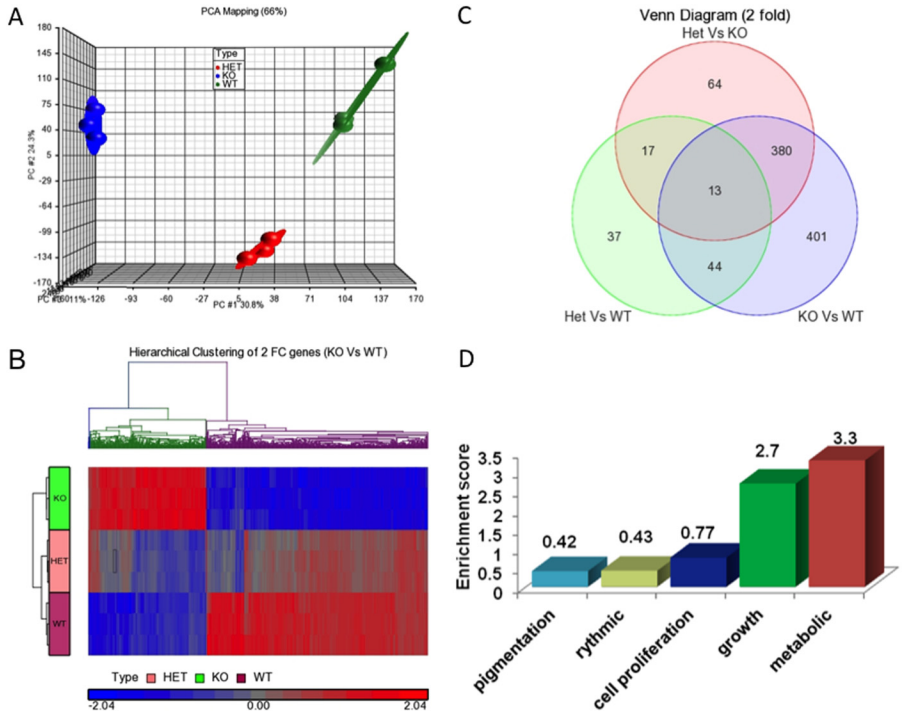

FIGURE 7. *A,* microarray data quality assessment using principal component analysis (*PCA*) shows replicate samples clustering in each genotype. *B,* hierarchical clustering of 838 genes that were found to be differentially expressed by 2-fold in WT *versus* KO MEFs. Each *row* represents a single sample in triplicate per genotype, and each column is a gene. *C,* overlap of statistically significant genes from each comparison are shown in the Venn diagram. The diagram shows the distribution of genes that are differentially expressed by 2-fold in all three groups ($p < 0.05\%$ and false discovery ratio of 0.01). *D,* Gene Ontology enrichment analysis of differentially expressed genes from the KO *versus* WT shows the high enrichment levels in genes associated with growth and metabolism.

the 838 transcripts (KO compared with WT) cluster into two distinct groups, although gene expression in HET was more similar to WT with few clusters shared with the KO group (Fig. 7*B*). Distribution of the differentially expressed genes in each comparison group is summarized in the Venn diagram in Fig. 7*C*. The 10 common transcripts present in all comparisons were *Oga*, *Scd2*, Lumican, *Gdf10*, Rho GTPase-activating protein 20 (*Arhgap20*), pleckstrin, *Cd36*, interferon-induced protein (*Ifit1*), Scavenger receptor class a member 5 (*Scara5*), and *Npl*. These microarray results confirmed the *Oga* deletion and showed that KO cells had a 4–19-fold reduction in *Oga* transcript levels as measured by five distinct sequence tags. Gene enrichment analysis was performed using the Gene Ontology database to examine the global transcriptional impact of the *Oga* loss of function. The 838 transcripts that differed in the KO *versus* WT animals showed the highest enrichment in genes associated with metabolism (Fig. 7*D*). Specifically, genes associated with glucose metabolism, lipid metabolism, sterol synthesis, cytokine signaling, innate immunity, and growth were most dramatically altered (Table 1). Although most of the genes known to be in these pathways were transcriptionally downregulated, approximately one-third were determined to be upregulated. Notably, using the Genomatix bioinformatics analysis tools, we found that the genes deregulated in HET MEFs have been associated with the development of sarcoma, obesity, neoplasms, and hypothyroidism. In particular, a module of genes linked to glucocorticoid-dependent regulation (Ncr3c1) of fat metabolism and obesity was over-represented in the genes differentially regulated in HET MEFs. This module regulates the hypothalamic pituitary adrenal axis.

Oga HET Animals Exhibit an Elevated Respiratory Exchange Ratio—To examine whether OGA deficiency causes changes in metabolism, we analyzed 13-week-old WT and HET female mice using the Comprehensive Lab Animal Monitoring System (CLAMS). These WT and HET mice exhibited similar body weight, food intake, energy expenditure, and physical activity (Table 2). To further characterize changes in metabolism, RER profiles in WT and HET mice were generated by taking measurements of O_2 consumption and CO_2 production (VCO_2/VO_2 ratios) in both light and dark cycles (to take into account any change in the activity of the animals due to the circadian clock). Measurement of RER in several light/dark cycles was performed after acclimatization as shown in Fig. 8*A*. Complete profiling was performed on these animals in three separate experiments as outlined under "Materials and Methods." The HET animals showed consistently higher RER values in both light and dark. Total RER measured over 24 h (Fig. 8*B*) showed a statistically significant increase from about 0.89 to 0.94. This increase was observed both in male and female HETs in three separate experiments after proper acclimatization to the metabolic chamber. An RER of 0.70 is indicative of oxidation of lipids as the predominant fuel source, whereas a value of 1.00 or above indicates that carbohydrates are being used as the main fuel source. Thus, the significantly increased RER observed in *Oga* HET animals suggests the preferential utilization of carbohydrates as opposed to lipids as the main source of fuel. This shift in RER to higher values suggests a global change in metabolism in the HET animals compared with their WT littermates.

TABLE 1

The genes that are observed to be differentially expressed, up or down, in microarray analysis studies were associated with metabolism and immunity

Selected transcripts from each group that were found to change more than 1.5-fold in *Oga* KO MEFs *versus* WT and their associated functional group are shown here.

Functional groups	Down regulated genes	Up regulated genes
Glucose metabolism	AldoC, Bcl2 Camkd1 Hk3, Igf1, Igfbp3, Igfbp4, Pik3r1,Gaa,Galnt6, Galnt4, Pygl,Agtr2	Ass1, Igfb7, Prkg2, Prkg1, Creb5, Slc2a9, Gfod1
Lipid Metabolism	Apoe, Apoc2, ApoBbec1, Acad10, Acss1, Cebpa, Cepbb, CD36, SLC27a1, Fabp7, Scd2, Plc ε1, Daglb, Pl d4 family m4, Mgll, Cyp4v3	Fabp3 (aP), Hmgcli, Acsl4, Slc33a1, Sorbs1,Dgkk
Sterol metabolism	Alox5ap, Ch25h, Hpgd, Rbp4, Crabp1, Hpgds, Hsd17b1, Hsd3b7, Hsdl1	
Calcium metabolism	Camk1d,Calcrl,Cacna2d3, Cadps,Dclk1	Casq2, Ccbe1, Cnn1
Cytokine signaling	Ccl12, MCP-1, Ccr5, Casp1, Socs2, Scocs3, Il18, , Il21r, Il6st, Cd14, Cd47, Cd48, Cd53, Cd68, Cd86,cd93, Stat1, Stat2, Sox9, Socs1, Socs2, Scos3, Tgfbi,Tgfbr3, Tnfrsf11b, Tnfrsf12a, Tnfrsf22	Il1rlike 1, Cd151,Cd24a,Cd40, Cd44, Cd55,Cd59a,Cx3cr1, Cxcl16, Cxcl15, Fas
Innate immunity	C1qa, C1qb,C3ar1,Ccl3, Ccl6, Ccl9, Ccr1, Ccr5	Ccl20
Growth and cell division	Cdkn1c, Cdkn2c, Csf1r, Csf2rb2, Eps8, Fgf18, Fgf21, Gas1, Gdf10,Gsn, Thra	Cdk6, Cdkn1a, Cdkn2b, Eif2a, Egr2 Fgf13, fgf5, Fgf9, Gadd45g, Gpr30, Gpr34, Gpr64, Hsp1b, Sdpr

TABLE 2

Metabolic parameters observed in 13-week-old WT and HET female mice maintained on a normal chow diet

Data were collected at 22 °C for 24 h after 2 days of adaptation to metabolic changers and are expressed at the mean ± S.E.

Parameter measured	WT ($n = 4$)	HET ($n = 5$)
Body weight (g)	24.3 ± 0.8	22.2 ± 2.9
TEE (kcal/mouse/day)	11.1 ± 0.3	9.8 ± 0.7
Food intake (kCa/mouse/h)	11.8 ± 0.6	12.8 ± 1.4
RER (VCO_2/VO_2)	0.89 ± 0.01	0.96 ± 0.02[a]
Total activity (beam brakes/min)	527 ± 55	352 ± 60

[a] $p < 0.05$.

Increased Body Weight Is Observed in Oga HET Females Fed a HFD—Growth and metabolic parameters were compared using age- and sex-matched mice from all genotypes. Metabolic parameters were measured at 8 weeks of age with mice on a regular diet, and at the 18th week all mice were switched to a HFD and evaluated up to the 26th week. HET male mice showed no changes in overall body weight, fat accumulation, or lean mass under normal or high fat diets (Fig. 9, *A*, *C*, and *E*, *left panels*). In contrast, HET females showed significantly increased weight gain compared with WT littermates (Fig. 9*B*, *right panel*). This weight gain was due both to significant elevated body fat accumulation (Fig. 9*D*, *right panel*) and lean mass accumulation in HET female mice relative to WT (Fig. 9*F*, *right panel*).

Serum Composition Changed in Oga HETs after HFD Feeding—There were no significant effects on serum parameters (*i.e.* glucose, insulin, triglyceride, or free fatty acid) in male or female mice under the normal chow diet (Table 3, part A). However, after 4 weeks of HFD feeding, HET and KO mice had detectable changes in key serum parameters. HET males showed significantly reduced blood glucose and circulating adiponectin levels compared with WT males (Table 3, part B). Interestingly, KO males also had lower blood glucose and significantly increased adiponectin levels together with elevated triglyceride, insulin, and serum leptin levels. HET females, however, demonstrated significantly increased circulating triglyceride, insulin, and leptin levels (Table 3, part B). In fact, both HET and KO females doubled their circulating insulin levels after being switched to the high fat diet but maintained blood glucose levels comparable with that of their WT littermates, suggesting the development of insulin resistance specifically in females. Markedly, increased serum leptin levels were observed, consistent with the extensive body fat accumulation in HET and KO females. In addition, elevated adiponectin levels were recorded for both HET and KO females, although HET males had significantly lower adiponectin levels than WT. Thus, the adiponectin, triglyceride, and insulin levels in HET mice exhibit a gender-biased difference consistent with increased adiposity in female HET animals.

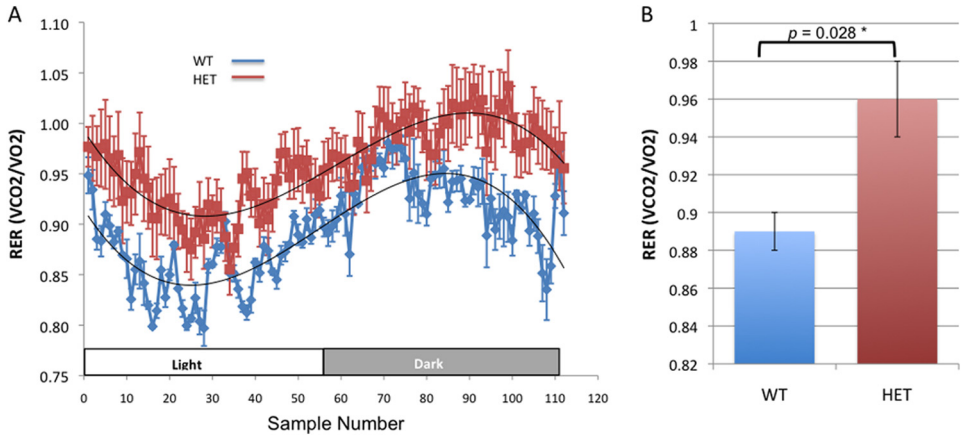

FIGURE 8. **Increases in RER values suggest a global change in metabolism in the HET animals compared with their WT littermates.** *A*, measurement of the VCO_2/VO_2 ratio in several light/dark cycles was performed after acclimatization (WT $n = 4$ and HET $n = 5$ animals). Data are represented as curve fit to the mean. *B*, HET animals showed consistently higher RER values in both light and dark cycles that reached statistical significance. Increases in total RER measured over 24 h were observed both in male and female HET mice.

Female HETs Achieve Glucose Tolerance by Increasing Insulin Secretion—No difference in glucose tolerance was observed in either male or female WT or HET mice when fed a normal diet (Fig. 10, *A–D*). Upon HFD feeding, HET males had improved glucose tolerance compared with WT males (Fig. 11*A*) with a notable increase in circulating insulin levels for both groups after being fed the HFD (Fig. 11*C*). In contrast, HET females had reduced glucose clearance with significantly elevated serum insulin (Fig. 11, *B* and *D*). HET female mice exhibited diminished glucose clearance capacity under HFD conditions compared with a normal diet, despite having elevated insulin levels. Gender difference is again apparent in insulin secretion and glucose control in HET animals as compared with their respective WT littermates, possibly correlated with adiposity. However, no differences in insulin tolerance were observed in HET male or female mice under normal or HFD conditions as compared with their WT littermates.

DISCUSSION

A previous study (48) examined *Oga* loss of function by gene-trap technology, and perinatal death of *Oga* KO pups within 24 h and genomic instability were reported. A follow-up study using these animals showed that *Oga* heterozygosity suppressed intestinal tumorigenesis in an established cancer model (49). Our studies using a conditional allele of *Oga* greatly extend these previous findings. Early expression of Cre recombinase in the murine zygote yielded HET and KO loss of function alleles of *Oga*. The resultant knock-out mice exhibit increased *O*-GlcNAcylation in both isolated MEF cells and tissues. Using a direct biochemical measurement of OGA activity in MEF cells, we noted a dramatic reduction in OGA activity in KO MEFs and a modest decrease in OGA activity in HET MEFs as compared with WT MEF levels. Unlike *Ogt* knock-out mice, which exhibit early embryonic lethality, the majority of *Oga* KO animals die within the perinatal period. About 89% of *Oga* KO pups were dead within 24–48 h after birth, suggesting a critical role of OGA function in the transition from birth to postpartum life. Hypoglycemia due to lowered glycogen storage has been previously linked to perinatal lethality (52), prompting us to examine postnatal glucose mobilization in these animals. We show here that the KO neonates have greatly reduced blood glucose that drops below the limit of detection after an 8-h starvation period. We also show that the neonatal liver in KO animals has greatly diminished glycogen stores. Thus, the perinatal lethality observed is likely due to defects in insulin-regulated glycogen accumulation and mobilization. Consistent with this, we observed dramatic increases in GSK3β Ser-9 phosphorylation in KO animals, consistent with a blunting of glycogen synthetase activity and the observed decreases in glycogen stores.

To examine other signaling pathways that may be altered, the MEFs derived from HET and KO lines were analyzed using whole genome microarray analysis. These data show dramatically altered expression of genes linked to cell metabolism and proliferation. Mice with a single functional *Oga* allele show alterations in pathways linked to increased fat mass and adipokine release, altered glucose tolerance, and increased insulin resistance. These HET animals also show significant elevation in total RER evident in both light and dark cycles of activity and respiratory monitoring. Metabolic phenotyping of this HET strain revealed a sexually dimorphic increase in fat mass upon exposure to a high fat diet. These metabolic phenotypes are more exaggerated in KO animals. We have significantly extended these finding by examining altered gene expression and metabolic signaling. Metabolic phenotyping of surviving KO mice revealed changes in insulin-glucose homeostasis and liver glycogen storage that may account for this perinatal lethal phenotype.

Oga Loss of Function Results in Deregulation of Genes Linked to Cell Proliferation and Metabolism—Whole genome analysis of expression revealed significant effects of the *Oga* deletion, lending notable insight into the roles of *O*-GlcNAc-dependent signaling. Gene ontogeny and pathway analysis revealed enrichment of differentially expressed genes linked to cell growth and metabolism. In HET animals, the deregulated transcription profiles were suggestive of metabolic disease, and alterations in genes associated with obesity were noted. Of particular note was deregulation of the gene Nr3c1 known to play a role in intrauterine programming of the hypothalamic pituitary adrenal axis. Nadler *et al.* (60) reported that obese mice show reduced expression of several adipogenic genes and some of

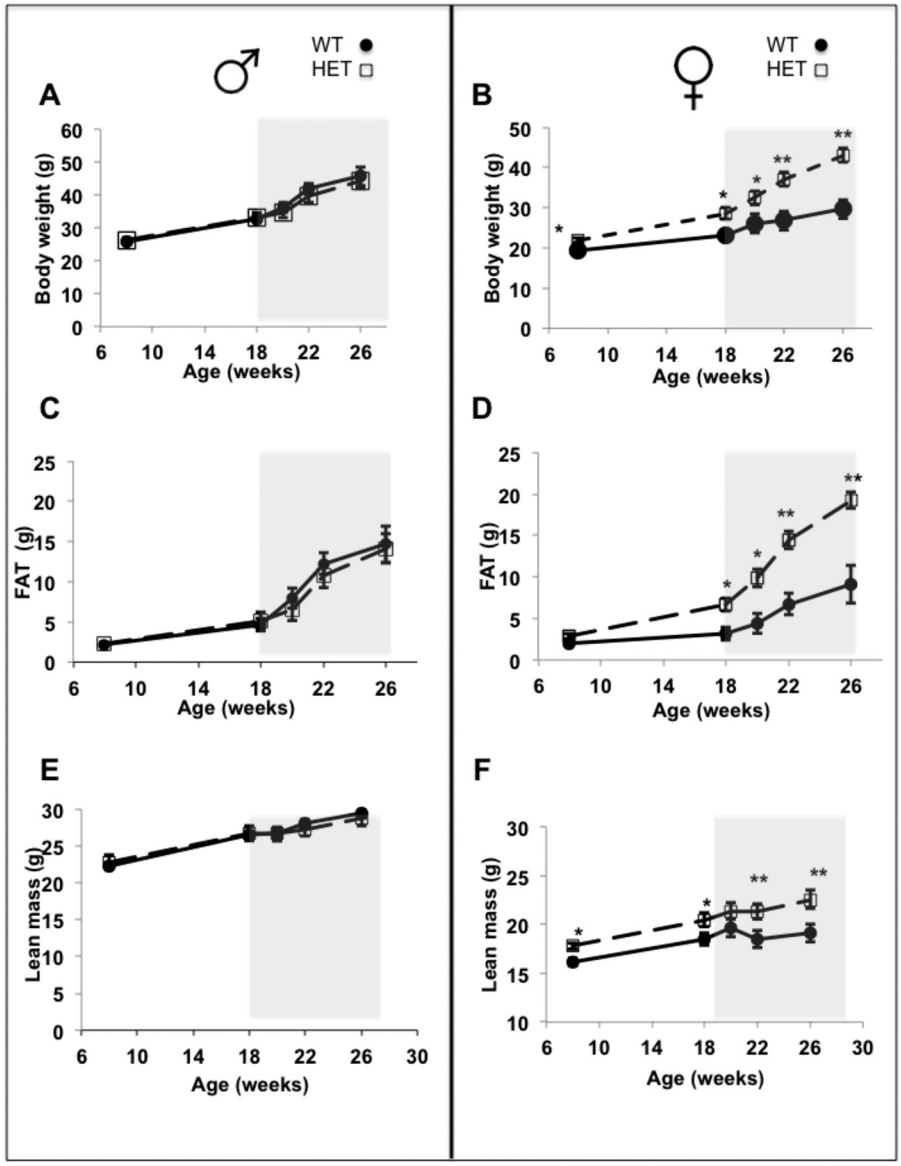

FIGURE 9. **Growth curves (*A* and *B*), fat (*C* and *D*), and lean mass composition (*E* and *F*) were determined in males (*left*) and in females (*right*) from 8 to 26 weeks of age.** Fat and lean mass were measured using an Echo MRI Bioanalyzer. Data are shown as mean ± S.E. using WT (females $n = 12$ males; $n = 15$) and HET (females $n = 29$ males $n = 18$). One-way ANOVA tests were used to determine statistical significance as follows: *, $p < 0.05$; **, $p < 0.01$. The *gray boxes* indicate the start of the 8-week HFD feeding period.

these (*e.g.* scd2, pcx, and Rbp4) were reduced in KO cell lines. In these KO animals, deregulated transcripts were enriched in genes associated with immunity and signaling. Inflammatory cytokine genes were also altered significantly in KO animals, suggesting possible changes in their immune function. Macrophage function has been recently identified as a prerequisite of early signals to adipose proliferation (61).

Perinatal Lethality and Metabolic Deregulation in Oga KO and HET Animals—Perinatal lethality can occur due to the malfunction of vital organs or the poor homeostasis of critical physiological functions. The 24–48-h post-partum window is a crucial time during which pups acclimate metabolically and physiologically following the removal of placental nutrition and oxygen supply. The KO pups in this study often died during this 24–48-h window without any growth or respiratory defect. *O*-GlcNAc cycling is known to modulate gene expression by associating with the transcriptome complex. In KO MEFs, the deregulation of *O*-GlcNAc cycling significantly reduced the expression of several genes, including *Scd2* (which was reduced by 10.96-fold) and *Cebpa* (which was reduced by 1.5-fold) The knock-out of either of these genes in mice results in neonatal lethality due to deficiencies in glucose homeostasis (52). We observe that the KO neonates are hypoglycemic compared with their WT or HET littermates and also have greatly reduced levels of liver glycogen. These findings suggest that the absence of *O*-GlcNAc cycling due to *Oga* loss of function may render the KO animals particularly susceptible to deficiencies in metabolic recovery after birth.

Altered Signaling Leads to Disruption in Insulin-Glucose Homeostasis—A number of molecular mechanisms have been proposed to explain why increased *O*-GlcNAc modification could exert negative effects on insulin signaling. These include

TABLE 3

Serum parameters measured in 8-week-old mice fed a normal diet (part A) and at 25–26 weeks of age after 4 weeks on a HFD (part B)

Female *Oga* HET mice ($n = 29$) had significantly higher insulin, triglycerides, and leptin levels compared with their WT ($n = 12$) littermates. *Oga* HET males ($n = 18$) had significantly reduced adiponectin levels compared with WT males ($n = 14$). In KO mice, both males and females ($n = 2$) show increased insulin and leptin levels. Data are presented as the mean ± S.E.; asterisks indicate significant differences relative to WT animals. A single asterisk represents $p < 0.05$ and a double asterisk represents $p < 0.01$, as determined by one-way ANOVA test. These are highlighted in red text.

A

8 weeks: Normal diet

Serum Parameter	WT male (n=15)	Het male (n=19)	KO male (n=2)	WT female (n=12)	Het female (n=29)	KO female (n=2)
Glucose(mg/dl)	145 ± 6	150 ± 8	143.5± 19	126 ± 7	126± 6	160 ± 41
Insulin (ng/ml)	0.92 ± 0.21	0.70 ± 0.07	0.7 ± 0	0.46 ± 0.07	0.52 ± 0.05	0.65 ± 0.19
Triglyceride (mg/dl)	102.6±9.7	88.4 ± 6.5	78.1 ± 7.0	79.0 ± 6.0	89.8 ± 6.3	103 .0 ± 9.0
FFA (mM)	0.56 ± 0.07	0.46 ± 0.04	0.5 ± 0	0.44 ± 0.07	0.49 ± 0.04	0.60 ± 0.14
Cholesterol (mg/dl)	98.6± 4.0	89.7 ± 3.2	82.9 ± 4.0	85.6 ± 3.7	88.5 ± 3.2	91 .0 ± 4.0

B

25-26 weeks: Last 4 weeks HFD

Serum parameter	WT male (n=14)	Het male (n=18)	KO male (n=2)	WT female (n=11)	Het female (n=29)	KO female (n=2)
Glucose(mg/dl)	177 ±11	148 ± 6*	129 ± 5	131 ± 11	140 ± 7	120 ± 47
Insulin (ng/ml)	8.9 ± 1.9	8.4 ± 2.2	18.0 ± 7.8	0.9 ± 0.23	2.7 ± 0.50*	2.9 ± 1.70
Triglyceride (mg/dl)	106 ± 7	109 ± 7	135 ± 31	64 ± 6	99 ± 8**	66 ± 22
FFA (mM)	0.62 ± 0.07	0.74 ± 0.06	0.47 ± 0.01	0.63 ± 0.04	0.71 ± 0.03	0.58 ± 0.02
Cholesterol (mg/dl)	165± 9	167 ± 9	134 ± 0.5	136 ± 6	147 ± 7	137 ± 10
Adiponectin (ug/ml)	9.4 ± 0.6	5.2 ± 1.2*	21.1± 8.2**	18.5 ± 1.3	24.7 ± 1.7	24.9 ± 12.9
Leptin (ng/ml)	40 ± 6.7	46 ± 3.8	59 ± 0.4	17 ± 5.8	47 ± 6.2*	53 ± 47.1

phosphatidylinositol 3-kinase inhibition (62), altered insulin secretion (63), and the reduction of AKT activity (64). The results of this study suggest that GSK3β may play a key role in lipid and glucose metabolism. Under basal conditions, GSK3β inhibits glycogen synthesis. Upon insulin stimulation, GSK3β is inhibited via phosphorylation at Ser-9. Notably, downstream of GSK3β is a cascade of metabolically relevant signaling pathways; these include pathways involved in insulin-mediated synthesis of both glycogen and fatty acids. The physiological effects of the elevated phosphorylation of GSK3β observed in the KO MEFs under basal conditions could mimic a condition of chronic insulin stimulation. Furthermore, the increased adiposity observed in KO mice could be a consequence of the deregulation of insulin-dependent macronutrient storage. Wang *et al.* (65) reported a complex downstream signaling effect upon *O*-GlcNAc-associated GSK3β inhibition in a cell-based model. HET female mice also demonstrated increased adiposity that gradually resulted in insulin resistance upon HFD feeding. It also appears that in response to increased adiposity, circulating leptin levels increased in these HET females. These findings are consistent with our previous report suggesting that OGT overexpression in muscle and fat under the GLUT4 promoter induced hyperleptinemia and insulin resistance in a sexually dimorphic fashion (54). Elevation of UDP-GlcNAc by glutamine fructose-6-phosphate amidotransferase overexpression induced a similar phenotype in mice (67–70) These findings and other studies suggest that adipokine changes associated with elevated *O*-GlcNAcylation in adipose tissues could be enough to trigger insulin resistance in other organs (71, 72).

Loss of *Oga* activity may also have direct effects on lipid storage in adipocytes. We have recently shown that *Oga* is an essential regulator of lipid droplet maintenance in adipocytes (17). By locally regulating the proteasome activity, the short isoform of OGA allows remodeling of the lipid droplet surface. Loss of *Oga* activity would be expected to interfere with lipid-droplet surface remodeling and may contribute to the observed obesity phenotype seen in KO animals.

Indirect Calorimetry Suggests Increased Carbohydrate Utilization of Carbohydrate Versus Lipid as Fuel—Our RER analysis suggests the *Oga* HET animals preferentially utilize carbohydrates rather than lipids as fuel. The biochemical basis for this finding remains unclear. The observed changes in insulin-triggered glycogen metabolism we have documented in these HET

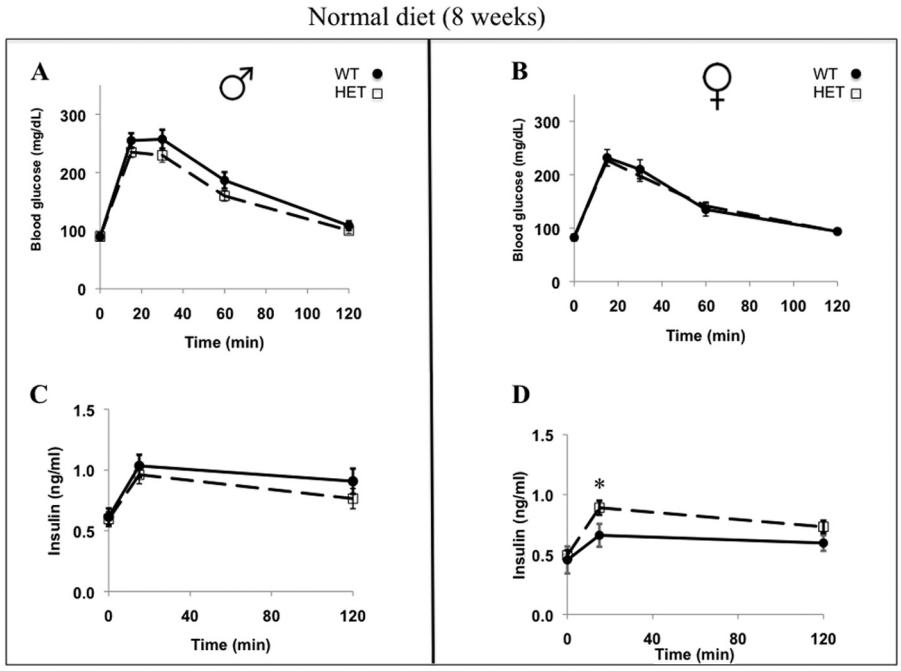

FIGURE 10. **Glucose tolerance test (*A* and *B*) and insulin levels (*C* and *D*) of WT and HET mice fed a normal diet at 8 weeks of age (WT (males $n = 15$; females $n = 12$) and HET mice (males $n = 18$; females $n = 29$)).** Data are presented as mean ± S.E., and statistical significance was calculated by one-way ANOVA test and is denoted by the *asterisk* ($p < 0.05$). Glucose tolerance tests were performed as described under "Materials and Methods."

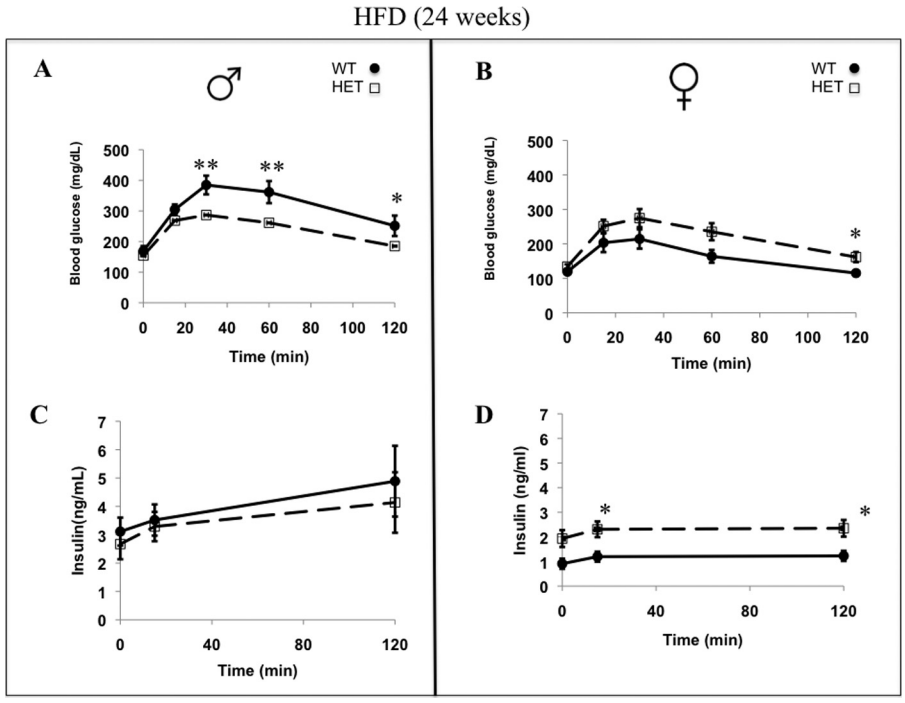

FIGURE 11. **Glucose tolerance test (*A* and *B*) and insulin levels (*C* and *D*) of WT and HET mice that had been fed a HFD for the previous 4 weeks at 24 weeks of age (WT (males $n = 15$; females $n = 12$) and HET mice (males $n = 18$; females $n = 29$)).** Data are presented as mean ± S.E., and statistical significance was calculated by one-way ANOVA test and is denoted by asterisks ($p < 0.05$). For glucose tolerance tests, animals were injected with 1 mg/g of body weight, and blood glucose was measured at the indicated time intervals.

animals are consistent with this observation. RER is a sensitive measure of metabolic rate and has been reported to be altered as the result of a number of loss of function mutations in the mouse (73–75). An increased basal metabolic rate and RER were observed in fat-specific insulin receptor knock-out mice (76). In an Akt1 knock-out model, mice exhibited elevated energy expenditure without an obvious increase in RER (75). Also, an adipose triacylglycerol lipase deletion was found to lead to an increase in the RER (74). In our *Oga* HET animals, the elevated RER is consistent with a global deregulation in both lipid and carbohydrate metabolism.

Sexual Dimorphism and Oga Loss of Function—Unlike *Oga* HET females, HET males did not develop obesity and were protected from diet-induced obesity. In this study, HET females had higher adiponectin levels compared with males. This supports the hypothesis that females tend to expand adipose tissue mass to alleviate insulin resistance. Adiponectin is known to promote insulin sensitivity through increased lipolysis (77) and altered signaling to store triglyceride in adipocytes to reduce triglyceride levels in liver and muscle (78). Interestingly, transgenic mice overexpressing glutamine fructose-6-phosphate amidotransferase in adipose tissue also exhibited gender-related differences in metabolic response. Specifically, females had lower glucose disposal rate, lower 2-deoxy-D-glucose uptake, and higher adiponectin levels than males (22).

Metabolic Homeostasis in a Genetically Controlled Developmental Model—There has been considerable controversy surrounding the role of *O*-GlcNAc cycling in the regulation of insulin-glucose homeostasis and metabolism. Genetic studies in *C. elegans* using null alleles of *ogt-1* and *oga-1* provided clear genetic evidence for a role of *O*-GlcNAc cycling in insulin signaling and insulin resistance (26, 33, 34, 38, 39, 79). Similar findings were obtained in *Drosophila* (43). In mammals, overexpression of OGT in muscle and fat was found to induce both insulin resistance and hyperleptinemia (54). Studies carried out in L1–3T3 cells showed that inhibition of OGA could render cells insulin-resistant (55). In addition, the insulin resistance of glycogen synthase was found to be mediated by the *O*-GlcNAc modification (80). Recently, studies in which adult mice or L1–3T3 cells were treated with cell-permeable OGA-selective inhibitors showed that this treatment did not induce insulin resistance (47, 81, 82). The work presented here suggests that in a developmental context, loss of OGA leads to many of the hallmarks of metabolic disease and a deregulation of glucose homeostasis in the intrauterine environment. This is quite distinct from acute inhibition of the enzyme in adult animals. Taken together, our findings suggest that OGA is required during development to maintain the essential aspects of metabolic homeostasis.

Summary—We have targeted the mouse *Oga (MGEA5*) locus for conditional disruption. The absence of the correlating mRNA, protein, and enzyme activity was observed in both MEFs and tissue from these animals. Whole genome gene expression analysis in MEFs showed notable deregulation of genes involved in immunity, cell proliferation, and metabolism. We observe constitutive activation of GSK3β and altered insulin responsiveness in both fetal and adult liver from *Oga* KO mice. Our metabolic results indicate increased adiposity associated with the development of insulin resistance in *Oga* HET females and KO mice in both genders. Increased dietary fat triggered adipose-mediated hyperleptinemia and hyperinsulinemia in *Oga* HET animals. Furthermore, *Oga* loss of function produces perinatal lethality associated with loss of glycogen accumulation in the fetal liver. Overall, the findings presented here suggest that although not essential, the OGA locus in the mouse is critical for the proper maintenance of insulin-glucose homeostasis, particularly in the intrauterine environment and the first few hours of life.

Acknowledgments—We are grateful to Dr. L. Hennighausen and Dr. G. Robinson at Laboratory of Genetics and Physiology, NIDDK, National Institutes of Health, for providing us with Cre transgenic mice. We acknowledge George Poy and Dr. Weiping Chen at NIDDK, National Institutes of Health, for microarray analysis and William Jou and Tatyana Chanturiya (NIDDK Mouse Metabolism Core Laboratory) for technical assistance with metabolic studies.

REFERENCES

1. Butkinaree, C., Park, K., and Hart, G. W. (2010) *O*-Linked β-*N*-acetylglucosamine (*O*-GlcNAc): Extensive crosstalk with phosphorylation to regulate signaling and transcription in response to nutrients and stress. *Biochim. Biophys. Acta* **1800,** 96–106
2. Ma, J., and Hart, G. W. (2014) *O*-GlcNAc profiling: from proteins to proteomes. *Clin. Proteomics* **11,** 8
3. Bond, M. R., and Hanover, J. A. (2013) *O*-GlcNAc cycling: a link between metabolism and chronic disease. *Annu. Rev. Nutr.* **33,** 205–229
4. Harwood, K. R., and Hanover, J. A. (2014) Nutrient-driven *O*-GlcNAc cycling–think globally but act locally. *J. Cell Sci.* **127,** 1857–1867
5. Lubas, W. A., Frank, D. W., Krause, M., and Hanover, J. A. (1997) *O*-Linked GlcNAc transferase is a conserved nucleocytoplasmic protein containing tetratricopeptide repeats. *J. Biol. Chem.* **272,** 9316–9324
6. Gao, Y., Wells, L., Comer, F. I., Parker, G. J., and Hart, G. W. (2001) Dynamic *O*-glycosylation of nuclear and cytosolic proteins: cloning and characterization of a neutral, cytosolic β-*N*-acetylglucosaminidase from human brain. *J. Biol. Chem.* **276,** 9838–9845
7. Hanover, J. A., Lai, Z., Lee, G., Lubas, W. A., and Sato, S. M. (1999) Elevated *O*-linked *N*-acetylglucosamine metabolism in pancreatic β-cells. *Arch. Biochem. Biophys.* **362,** 38–45
8. Hanover, J. A. (2001) Glycan-dependent signaling: *O*-linked *N*-acetylglucosamine. *FASEB J.* **15,** 1865–1876
9. Slawson, C., and Hart, G. W. (2003) Dynamic interplay between *O*-GlcNAc and *O*-phosphate: the sweet side of protein regulation. *Curr. Opin. Struct. Biol.* **13,** 631–636
10. Slawson, C., Copeland, R. J., and Hart, G. W. (2010) *O*-GlcNAc signaling: a metabolic link between diabetes and cancer? *Trends Biochem. Sci.* **35,** 547–555
11. Marshall, S. (2006) Role of insulin, adipocyte hormones, and nutrient-sensing pathways in regulating fuel metabolism and energy homeostasis: a nutritional perspective of diabetes, obesity, and cancer. *Sci. STKE* 2006, re7
12. Love, D. C., and Hanover, J. A. (2005) The hexosamine signaling pathway: deciphering the "*O*-GlcNAc code". *Sci. STKE* 2005, re13
13. Heckel, D., Comtesse, N., Brass, N., Blin, N., Zang, K. D., and Meese, E. (1998) Novel immunogenic antigen homologous to hyaluronidase in meningioma. *Hum. Mol. Genet.* **7,** 1859–1872
14. Comtesse, N., Maldener, E., and Meese, E. (2001) Identification of a nuclear variant of MGEA5, a cytoplasmic hyaluronidase and a β-*N*-acetylglucosaminidase. *Biochem. Biophys. Res. Commun.* **283,** 634–640
15. Zachara, N. E., and Hart, G. W. (2004) *O*-GlcNAc a sensor of cellular state: the role of nucleocytoplasmic glycosylation in modulating cellular function in response to nutrition and stress. *Biochim. Biophys. Acta* **1673,** 13–28
16. Schultz, J., and Pils, B. (2002) Prediction of structure and functional residues for *O*-GlcNAcase, a divergent homologue of acetyltransferases. *FEBS Lett.* **529,** 179–182
17. Keembiyehetty, C. N., Krzeslak, A., Love, D. C., and Hanover, J. A. (2011) A lipid-droplet-targeted *O*-GlcNAcase isoform is a key regulator of the proteasome. *J. Cell Sci.* **124,** 2851–2860
18. Duggirala, R., Blangero, J., Almasy, L., Dyer, T. D., Williams, K. L., Leach, R. J., O'Connell, P., and Stern, M. P. (1999) Linkage of type 2 diabetes mellitus and of age at onset to a genetic location on chromosome 10q in Mexican Americans. *Am. J. Hum. Genet.* **64,** 1127–1140
19. Farook, V. S., Bogardus, C., and Prochazka, M. (2002) Analysis of MGEA5 on 10q24.1-q24.3 encoding the β-*O*-linked *N*-acetylglucosaminidase as a

candidate gene for type 2 diabetes mellitus in Pima Indians. *Mol. Genet. Metab.* **77,** 189–193
20. Lehman, D. M., Fu, D. J., Freeman, A. B., Hunt, K. J., Leach, R. J., Johnson-Pais, T., Hamlington, J., Dyer, T. D., Arya, R., Abboud, H., Göring, H. H., Duggirala, R., Blangero, J., Konrad, R. J., and Stern, M. P. (2005) A single nucleotide polymorphism in MGEA5 encoding *O*-GlcNAc-selective *N*-acetyl-β-D-glucosaminidase is associated with type 2 diabetes in Mexican Americans. *Diabetes* **54,** 1214–1221
21. Kudlow, J. E. (2002) The *O*-GlcNAcase theory of diabetes: commentary on a candidate gene for diabetes. *Mol. Genet. Metab.* **77,** 1–2
22. McClain, D. A. (2002) Hexosamines as mediators of nutrient sensing and regulation in diabetes. *J. Diabetes Complications* **16,** 72–80
23. Issad, T., and Kuo, M. (2008) *O*-GlcNAc modification of transcription factors, glucose sensing and glucotoxicity. *Trends Endocrinol. Metab.* **19,** 380–389
24. Hanover, J. A., Krause, M. W., and Love, D. C. (2010) The hexosamine signaling pathway: *O*-GlcNAc cycling in feast or famine. *Biochim. Biophys. Acta* **1800,** 80–95
25. Love, D. C., Krause, M. W., and Hanover, J. A. (2010) *O*-GlcNAc cycling: emerging roles in development and epigenetics. *Semin. Cell Dev. Biol.* **21,** 646–654
26. Love, D. C., Ghosh, S., Mondoux, M. A., Fukushige, T., Wang, P., Wilson, M. A., Iser, W. B., Wolkow, C. A., Krause, M. W., and Hanover, J. A. (2010) Dynamic *O*-GlcNAc cycling at promoters of *Caenorhabditis elegans* genes regulating longevity, stress, and immunity. *Proc. Natl. Acad. Sci. U.S.A.* **107,** 7413–7418
27. Ranuncolo, S. M., Ghosh, S., Hanover, J. A., Hart, G. W., and Lewis, B. A. (2012) Evidence of the involvement of *O*-GlcNAc-modified human RNA polymerase II CTD in transcription *in vitro* and *in vivo*. *J. Biol. Chem.* **287,** 23549–23561
28. Shafi, R., Iyer, S. P., Ellies, L. G., O'Donnell, N., Marek, K. W., Chui, D., Hart, G. W., and Marth, J. D. (2000) The *O*-GlcNAc transferase gene resides on the X chromosome and is essential for embryonic stem cell viability and mouse ontogeny. *Proc. Natl. Acad. Sci. U.S.A.* **97,** 5735–5739
29. O'Donnell, N., Zachara, N. E., Hart, G. W., and Marth, J. D. (2004) Ogt-dependent X-chromosome-linked protein glycosylation is a requisite modification in somatic cell function and embryo viability. *Mol. Cell. Biol.* **24,** 1680–1690
30. Hanover, J. A., Yu, S., Lubas, W. B., Shin, S. H., Ragano-Caracciola, M., Kochran, J., and Love, D. C. (2003) Mitochondrial and nucleocytoplasmic isoforms of *O*-linked GlcNAc transferase encoded by a single mammalian gene. *Arch. Biochem. Biophys.* **409,** 287–297
31. Abramowitz, L. K., Olivier-Van Stichelen, S., and Hanover, J. A. (2014) Chromosome imbalance as a driver of sex disparity in disease. *J. Genomics* **2,** 77–88
32. Olivier-Van Stichelen, S., Abramowitz, L. K., and Hanover, J. A. (2014) X marks the spot: Does it matter that *O*-GlcNAc Transferase is an X-linked gene? *Biochem. Biophys. Res. Commun.* **453,** 201–207
33. Forsythe, M. E., Love, D. C., Lazarus, B. D., Kim, E. J., Prinz, W. A., Ashwell, G., Krause, M. W., and Hanover, J. A. (2006) *Caenorhabditis elegans* ortholog of a diabetes susceptibility locus: oga-1 (*O*-GlcNAcase) knockout impacts *O*-GlcNAc cycling, metabolism, and dauer. *Proc. Natl. Acad. Sci. U.S.A.* **103,** 11952–11957
34. Hanover, J. A., Forsythe, M. E., Hennessey, P. T., Brodigan, T. M., Love, D. C., Ashwell, G., and Krause, M. (2005) A *Caenorhabditis elegans* model of insulin resistance: altered macronutrient storage and dauer formation in an OGT-1 knockout. *Proc. Natl. Acad. Sci. U.S.A.* **102,** 11266–11271
35. Hanover, J. A., and Wang, P. (2013) *O*-GlcNAc cycling shows neuroprotective potential in *C. elegans* models of neurodegenerative disease. *Worm* **2,** e27043
36. Mondoux, M. A., Love, D. C., Ghosh, S. K., Fukushige, T., Bond, M., Weerasinghe, G. R., Hanover, J. A., and Krause, M. W. (2011) *O*-Linked-*N*-acetylglucosamine cycling and insulin signaling are required for the glucose stress response in *Caenorhabditis elegans*. *Genetics* **188,** 369–382
37. Radermacher, P. T., Myachina, F., Bosshardt, F., Pandey, R., Mariappa, D., Müller, H. A., and Lehner, C. F. (2014) *O*-GlcNAc reports ambient temperature and confers heat resistance on ectotherm development. *Proc. Natl. Acad. Sci. U.S.A.* **111,** 5592–5597
38. Wang, P., Lazarus, B. D., Forsythe, M. E., Love, D. C., Krause, M. W., and Hanover, J. A. (2012) *O*-GlcNAc cycling mutants modulate proteotoxicity in *Caenorhabditis elegans* models of human neurodegenerative diseases. *Proc. Natl. Acad. Sci. U.S.A.* **109,** 17669–17674
39. Wang, P., and Hanover, J. A. (2013) Nutrient-driven *O*-GlcNAc cycling influences autophagic flux and neurodegenerative proteotoxicity. *Autophagy* **9,** 604–606
40. Gambetta, M. C., Oktaba, K., and Müller, J. (2009) Essential role of the glycosyltransferase sxc/Ogt in polycomb repression. *Science* **325,** 93–96
41. Ingham, P. W. (1984) A gene that regulates the bithorax complex differentially in larval and adult cells of *Drosophila*. *Cell* **37,** 815–823
42. Sinclair, D. A., Syrzycka, M., Macauley, M. S., Rastgardani, T., Komljenovic, I., Vocadlo, D. J., Brock, H. W., and Honda, B. M. (2009) *Drosophila O*-GlcNAc transferase (OGT) is encoded by the Polycomb group (PcG) gene, super sex combs (sxc). *Proc. Natl. Acad. Sci. U.S.A.* **106,** 13427–13432
43. Sekine, O., Love, D. C., Rubenstein, D. S., and Hanover, J. A. (2010) Blocking *O*-linked GlcNAc cycling in *Drosophila* insulin-producing cells perturbs glucose-insulin homeostasis. *J. Biol. Chem.* **285,** 38684–38691
44. Kim, E. J., Perreira, M., Thomas, C. J., and Hanover, J. A. (2006) An *O*-GlcNAcase-specific inhibitor and substrate engineered by the extension of the *N*-acetyl moiety. *J. Am. Chem. Soc.* **128,** 4234–4235
45. Kim, E. J., Amorelli, B., Abdo, M., Thomas, C. J., Love, D. C., Knapp, S., and Hanover, J. A. (2007) Distinctive inhibition of *O*-GlcNAcase isoforms by an α-GlcNAc thiolsulfonate. *J. Am. Chem. Soc.* **129,** 14854–14855
46. Kim, E. J., Bond, M. R., Love, D. C., and Hanover, J. A. (2014) Chemical tools to explore nutrient-driven *O*-GlcNAc cycling. *Crit. Rev. Biochem. Mol. Biol.* **49,** 327–342
47. Macauley, M. S., Bubb, A. K., Martinez-Fleites, C., Davies, G. J., and Vocadlo, D. J. (2008) Elevation of global *O*-GlcNAc levels in 3T3-L1 adipocytes by selective inhibition of *O*-GlcNAcase does not induce insulin resistance. *J. Biol. Chem.* **283,** 34687–34695
48. Yang, Y. R., Song, M., Lee, H., Jeon, Y., Choi, E. J., Jang, H. J., Moon, H. Y., Byun, H. Y., Kim, E. K., Kim, D. H., Lee, M. N., Koh, A., Ghim, J., Choi, J. H., Lee-Kwon, W., *et al.* (2012) *O*-GlcNAcase is essential for embryonic development and maintenance of genomic stability. *Aging Cell* **11,** 439–448
49. Yang, Y. R., Jang, H. J., Yoon, S., Lee, Y. H., Nam, D., Kim, I. S., Lee, H., Kim, H., Choi, J. H., Kang, B. H., Ryu, S. H., and Suh, P. G. (2014) OGA heterozygosity suppresses intestinal tumorigenesis in Apc(min/+) mice. *Oncogenesis* **3,** e109
50. Nagy, A. (2000) Cre recombinase: the universal reagent for genome tailoring. *Genesis* **26,** 99–109
51. Babinet, C., and Cohen-Tannoudji, M. (2001) Genome engineering via homologous recombination in mouse embryonic stem (ES) cells: an amazingly versatile tool for the study of mammalian biology. *An. Acad. Bras. Cienc.* **73,** 365–383
52. Turgeon, B., and Meloche, S. (2009) Interpreting neonatal lethal phenotypes in mouse mutants: insights into gene function and human diseases. *Physiol. Rev.* **89,** 1–26
53. Kim, E. J., Kang, D. O., Love, D. C., and Hanover, J. A. (2006) Enzymatic characterization of *O*-GlcNAcase isoforms using a fluorogenic GlcNAc substrate. *Carbohydr. Res.* **341,** 971–982
54. McClain, D. A., Lubas, W. A., Cooksey, R. C., Hazel, M., Parker, G. J., Love, D. C., and Hanover, J. A. (2002) Altered glycan-dependent signaling induces insulin resistance and hyperleptinemia. *Proc. Natl. Acad. Sci. U.S.A.* **99,** 10695–10699
55. Vosseller, K., Wells, L., Lane, M. D., and Hart, G. W. (2002) Elevated nucleocytoplasmic glycosylation by *O*-GlcNAc results in insulin resistance associated with defects in Akt activation in 3T3-L1 adipocytes. *Proc. Natl. Acad. Sci. U.S.A.* **99,** 5313–5318
56. Eldar-Finkelman, H., Schreyer, S. A., Shinohara, M. M., LeBoeuf, R. C., and Krebs, E. G. (1999) Increased glycogen synthase kinase-3 activity in diabetes- and obesity-prone C57BL/6J mice. *Diabetes* **48,** 1662–1666
57. Summers, S. A., Kao, A. W., Kohn, A. D., Backus, G. S., Roth, R. A., Pessin, J. E., and Birnbaum, M. J. (1999) The role of glycogen synthase kinase 3β in insulin-stimulated glucose metabolism. *J. Biol. Chem.* **274,** 17934–17940
58. Oreña, S. J., Torchia, A. J., and Garofalo, R. S. (2000) Inhibition of glycogen-synthase kinase 3 stimulates glycogen synthase and glucose transport

by distinct mechanisms in 3T3-L1 adipocytes. *J. Biol. Chem.* **275,** 15765–15772
59. Doble, B. W., and Woodgett, J. R. (2003) GSK-3: tricks of the trade for a multi-tasking kinase. *J. Cell Sci.* **116,** 1175–1186
60. Nadler, S. T., Stoehr, J. P., Schueler, K. L., Tanimoto, G., Yandell, B. S., and Attie, A. D. (2000) The expression of adipogenic genes is decreased in obesity and diabetes mellitus. *Proc. Natl. Acad. Sci. U.S.A.* **97,** 11371–11376
61. Fuentes, L., Roszer, T., and Ricote, M. (2010) Inflammatory mediators and insulin resistance in obesity: role of nuclear receptor signaling in macrophages. *Mediators Inflamm.* 2010, 219583
62. Yang, X., Ongusaha, P. P., Miles, P. D., Havstad, J. C., Zhang, F., So, W. V., Kudlow, J. E., Michell, R. H., Olefsky, J. M., Field, S. J., and Evans, R. M. (2008) Phosphoinositide signalling links *O*-GlcNAc transferase to insulin resistance. *Nature* **451,** 964–969
63. Akimoto, Y., Hart, G. W., Wells, L., Vosseller, K., Yamamoto, K., Munetomo, E., Ohara-Imaizumi, M., Nishiwaki, C., Nagamatsu, S., Hirano, H., and Kawakami, H. (2007) Elevation of the post-translational modification of proteins by *O*-linked *N*-acetylglucosamine leads to deterioration of the glucose-stimulated insulin secretion in the pancreas of diabetic Goto-Kakizaki rats. *Glycobiology* **17,** 127–140
64. Soesanto, Y. A., Luo, B., Jones, D., Taylor, R., Gabrielsen, J. S., Parker, G., and McClain, D. A. (2008) Regulation of Akt signaling by *O*-GlcNAc in euglycemia. *Am. J. Physiol. Endocrinol. Metab.* **295,** E974–E980
65. Wang, Z., Pandey, A., and Hart, G. W. (2007) Dynamic interplay between *O*-linked *N*-acetylglucosaminylation and glycogen synthase kinase-3-dependent phosphorylation. *Mol. Cell. Proteomics* **6,** 1365–1379
66. Chen, M., Berger, A., Kablan, A., Zhang, J., Gavrilova, O., and Weinstein, L. S. (2012) Gsα deficiency in the paraventricular nucleus of the hypothalamus partially contributes to obesity associated with Gsα mutations. *Endocrinology* **153,** 4256–4265
67. Cooksey, R. C., and McClain, D. A. (2002) Transgenic mice overexpressing the rate-limiting enzyme for hexosamine synthesis in skeletal muscle or adipose tissue exhibit total body insulin resistance. *Ann. N.Y. Acad. Sci.* **967,** 102–111
68. McClain, D. A., Alexander, T., and Cooksey, R. C. (2000) Hexosamines stimulate leptin production in transgenic mice. *Endocrinology* **141,** 1999–2002
69. McClain, D. A., Hazel, M., and Parker, G. (2005) Adipocytes with increased hexosamine flux exhibit insulin resistance, increased glucose uptake, and increased synthesis and storage of lipid. *Am. J. Physiol. Endocrinol. Metab.* **288,** E973–E979
70. Hazel, M., Cooksey, R. C., Jones, D., Parker, G., Neidigh, J. L., Witherbee, B., Gulve, E. A., and McClain, D. A. (2004) Activation of the hexosamine signaling pathway in adipose tissue results in decreased serum adiponectin and skeletal muscle insulin resistance. *Endocrinology* **145,** 2118–2128
71. Müller, G., Ertl, J., Gerl, M., and Preibisch, G. (1997) Leptin impairs metabolic actions of insulin in isolated rat adipocytes. *J. Biol. Chem.* **272,** 10585–10593
72. Teo, C. F., Wollaston-Hayden, E. E., and Wells, L. (2010) Hexosamine flux, the *O*-GlcNAc modification, and the development of insulin resistance in adipocytes. *Mol. Cell. Endocrinol.* **318,** 44–53
73. Benz, V., Bloch, M., Wardat, S., Böhm, C., Maurer, L., Mahmoodzadeh, S., Wiedmer, P., Spranger, J., Foryst-Ludwig, A., and Kintscher, U. (2012) Sexual dimorphic regulation of body weight dynamics and adipose tissue lipolysis. *PLoS One* **7,** e37794
74. Huijsman, E., van de Par, C., Economou, C., van der Poel, C., Lynch, G. S., Schoiswohl, G., Haemmerle, G., Zechner, R., and Watt, M. J. (2009) Adipose triacylglycerol lipase deletion alters whole body energy metabolism and impairs exercise performance in mice. *Am. J. Physiol. Endocrinol. Metab.* **297,** E505–E513
75. Wan, M., Easton, R. M., Gleason, C. E., Monks, B. R., Ueki, K., Kahn, C. R., and Birnbaum, M. J. (2012) Loss of Akt1 in mice increases energy expenditure and protects against diet-induced obesity. *Mol. Cell. Biol.* **32,** 96–106
76. Katic, M., Kennedy, A. R., Leykin, I., Norris, A., McGettrick, A., Gesta, S., Russell, S. J., Bluher, M., Maratos-Flier, E., and Kahn, C. R. (2007) Mitochondrial gene expression and increased oxidative metabolism: role in increased lifespan of fat-specific insulin receptor knock-out mice. *Aging Cell* **6,** 827–839
77. Qiao, L., Kinney, B., Schaack, J., and Shao, J. (2011) Adiponectin inhibits lipolysis in mouse adipocytes. *Diabetes* **60,** 1519–1527
78. Kim, J. Y., van de Wall, E., Laplante, M., Azzara, A., Trujillo, M. E., Hofmann, S. M., Schraw, T., Durand, J. L., Li, H., Li, G., Jelicks, L. A., Mehler, M. F., Hui, D. Y., Deshaies, Y., Shulman, G. I., Schwartz, G. J., and Scherer, P. E. (2007) Obesity-associated improvements in metabolic profile through expansion of adipose tissue. *J. Clin. Invest.* **117,** 2621–2637
79. Rahman, M. M., Stuchlick, O., El-Karim, E. G., Stuart, R., Kipreos, E. T., and Wells, L. (2010) Intracellular protein glycosylation modulates insulin mediated lifespan in *C. elegans*. *Aging* **2,** 678–690
80. Parker, G. J., Lund, K. C., Taylor, R. P., and McClain, D. A. (2003) Insulin resistance of glycogen synthase mediated by *O*-linked *N*-acetylglucosamine. *J. Biol. Chem.* **278,** 10022–10027
81. Macauley, M. S., Shan, X., Yuzwa, S. A., Gloster, T. M., and Vocadlo, D. J. (2010) Elevation of global *O*-GlcNAc in rodents using a selective *O*-GlcNAcase inhibitor does not cause insulin resistance or perturb glucohomeostasis. *Chem. Biol.* **17,** 949–958
82. Macauley, M. S., He, Y., Gloster, T. M., Stubbs, K. A., Davies, G. J., and Vocadlo, D. J. (2010) Inhibition of *O*-GlcNAcase using a potent and cell-permeable inhibitor does not induce insulin resistance in 3T3-L1 adipocytes. *Chem. Biol.* **17,** 937–948
83. Wagner, K. U., McAllister, K., Ward, T., Davis, B., Wiseman, R., and Hennighausen, L. (2001) Spatial and temporal expression of the Cre gene under the control of the MMTV-LTR in different lines of transgenic mice. *Transgenic Res.* **10,** 545–553
84. Miller, S. A., Dykes, D. D., and Polesky, H. F. (1988) A simple salting out procedure for extracting DNA from human nucleated cells. *Nucleic Acids Res.* **16,** 1215